REPUBLIC OF TURKEY

YILDIZ TECHNICAL UNIVERSITY

GRADUATE SCHOOL OF SCIENCE AND ENGINEERING

ANTIREFLECTION COATINGS BASED ON SILICA-POLYNORBORNENE NANOCOMPOSITES

Olcay İrem İREY

MASTER OF SCIENCE THESIS

Department of Chemistry

Physical Chemistry Program

Supervisor

Prof. Dr. Tarık EREN

Co-Supervisor

Dr. Refika BUDAKOĞLU

February, 2023

REPUBLIC OF TURKEY

YILDIZ TECHNICAL UNIVERSITY

GRADUATE SCHOOL OF SCIENCE AND ENGINEERING

ANTIREFLECTION COATINGS BASED ON SILICA-POLYNORBORNENE NANOCOMPOSITES

A thesis submitted by Olcay İrem İREY in partial fulfillment of the requirements for the degree of MASTER is approved by the committee on 15.02.2023 in Department of Chemistry, Physical Chemistry Program.

Prof. Dr. Tarık EREN Yıldız Technical University Supervisor	Dr. Refika BUDAKOĞLU Co- supervisor

Approved By the Examining Committee

Prof. Dr. Tarık EREN, Supervisor
Yildiz Technical University _____

Assoc. Prof. Dr. Dolunay ŞAKAR DAŞDAN, Member
Yildiz Technical University _____

Prof. Dr. Ayşe Neren ÖKTE, Member
Bogazici University _____

I hereby declare that I have obtained the required legal permissions during data collection and exploitation procedures, that I have made the in-text citations and cited the references properly, that I haven't falsified and/or fabricated research data and results of the study and that I have abided by the principles of the scientific research and ethics during my Thesis Study under the title of Antireflection Coatings Based on Silica-Polynorbornene Nanocomposites supervised by my supervisor, Prof. Dr. Tarık EREN. In the case of a discovery of false statement, I am to acknowledge any legal consequence.

Olcay İrem İREY

Signature

In memory of my beloved father Muzaffer İREY,

ACKNOWLEDGMENTS

I would like to express my sincere thanks to my esteemed advisor Prof. Dr. Tarık EREN, who shared his valuable knowledge and experience with me throughout my graduate education, and to my co-advisor, Chief Researcher Dr. Refika BUDAKOĞLU, for whom I felt very lucky to have crossed paths at the very beginning of my career journey.

I would like to thank Haluk ERDEM, Director of Atmospheric Coating Technologies, who supported me in carrying out my graduate studies.

While completing my thesis, I further thank to Prof. Dr. Markus GALLEI from Saarland University, Chief Researcher Şener YILMAZ from Şişecam Science Technology and Design Center and Prof. Dr. Serap DERMAN and Assoc. Prof. Dr. Murat TOPUZOĞULLARI from Yıldız Technical University Bioengineering Department for their support in some of the analysis. I also thank to all members of Eren Research Group it has been a great pleasure to be a part of this group.

Some of the experimental studies, analysis, testing and characterizations were carried out at Şişecam Science Technology and Design Center, which I am proud to work at. I would like to thank all Şişecam Science Technology and Design Center employees, especially the Atmospheric Coating Technologies Directorate, for their support in my thesis work. I further thank to Gizem AYDIN SOBACI, Zeynep AYDIN and Deniz AVCI for their support and advices during the writing process of my thesis.

I would like to thank my beloved mother Rahime İREY, my father Muzaffer İREY, and my siblings Ali Onur Can İREY, Merih Gencay İREY and my dearest one Aylin İdil İREY, who have supported me throughout my life and made me who I am today.

I would like to express my sincere thanks to Samed BOZDOĞAN for his caring love and holding my hand for life no matter what. I finally thank to all my friends who trusted me and stood by me.

Olcay İrem İREY

TABLE OF CONTENTS

LIST OF SYMBOLS viii

LIST OF ABBREVIATIONS ix

LIST OF FIGURES xi

LIST OF TABLES xiv

ABSTRACT xv

ÖZET xvi

1 INTRODUCTION 1

1.1 Literature Review 1

1.1.1 Hollow Sphere Nanoparticle 3

1.2 Objective of the Thesis 7

1.3 Hypothesis 8

2 ANTI-REFLECTION 9

2.1 What is Anti-reflection 9

2.2 PV Module with AR-Coated Glass 11

3 SOL-GEL COATING METHODS 12

3.1 Spin Coating 12

3.2 Spray Coating 13

3.3 Dip-Coating 13

4 SOL-GEL METHOD 15

4.1 Advantages and Disadvantages of Sol-gel Method 15

4.2 Critical Parameters of Sol-Gel 16

4.2.1 Precursors 16

4.2.2 pH/Catalysts 17

4.2.3 The H_2O/Alkoxy Molar Ratio 18

4.2.4 Temperature 18

4.3 Reaction Mechanism 19

4.4 Stöber Process 20

5 POLYMERS 22

5.1 Controlled Polymerization 24

5.2 Ring-Opening Metathesis Polymerization (ROMP) 24

6 EXPERIMENTAL 28

6.1 Materials & Methods 28
6.1.1 Used Chemicals 28
6.1.2 Used Equipment and Devices 28
6.2 Method 28
6.3 Synthesis of Monomers 29
6.3.1 Synthesis of (1R,2S,6R,7R)-4-oxatricyclo [5.2.1.$0^{2,6}$] dec-8-ene-3,5-dione 29
6.3.2 Synthesis of (2R,6S)-4-oxatricyclo [5.2.1.$0^{2,6}$] dec-8-ene-3,5-dione (Monomer 1) 29
6.3.3 Synthesis of Furan Maleic Anhydride Diels Alder Product (4,10-Dioxa-tricyclo [5.2.1.$0^{2,6}$] dec-8-ene-3,5-dione) (Monomer 2) 30
6.3.4 Synthesis of Grubbs 3rd Generation Catalyst 30
6.4 Polymerizations of Norbornene Monomers with ROMP 30
6.5 Synthesis of Polymers 31
6.5.1 Synthesis of Exo-Norbornene Polymer (Poly1-5k and Poly1-10k) 31
6.5.2 Synthesis of Oxanorbornene Polymer (Poly2-5k and Poly2-10k) 31
6.6 Hydrolysis of Polymers 32
6.7 Sol-Gel Synthesis with Produced Polymers 32
6.8 Coating with Produced Sol-Gels 33
7 RESULTS AND DISCUSSION 35
7.1 Synthesis and Characterization of Monomers 35
7.1.1 Synthesis of (1R,2S,6R,7R)-4-oxatricyclo [5.2.1.$0^{2,6}$] dec-8-ene-3,5- dione 35
7.1.2 Synthesis of (2R,6S)-4-oxatricyclo [5.2.1.$0^{2,6}$] dec-8-ene-3,5-dione (Monomer 1) 35
7.1.3 Synthesis of Furan Maleic Anhydride Diels Alder Product (4,10-Dioxa-tricyclo [5.2.1.0] dec-8-ene-3,5-dione) (Monomer 2) 38
7.2 Synthesis and Characterization of Polymers 40
7.2.1 Synthesis of Exo-Adducted Norbornene Polymer (Poly1-5k and Poly1-10k) 40
7.2.2 Synthesis of Oxanorbornene Polymer (Poly2-5k and Poly2-10k) 46
7.2.3 Molecular Weight Distribution of Polymers 52
7.2.4 Thermal Properties of Synthesized Polymers 53
7.3 Sol-Gel Synthesis and Characterization with Hydrolysed Polymers 54
7.3.1 Sol-gel Synthesis (Sol1-5k, Sol1-10k, Sol2-5k, Sol2-10k) 54

7.3.2 Nanoparticles Size Distribution via DLS 55
7.4 Coating with Produced Sol-Gels 63
7.4.1 Dip-coating Procedure with Produced Sol-Gels 63
7.4.2 Characterization of Coated Glasses 64
7.5 Conclusion 68
REFERENCES **70**
PUBLICATIONS FROM THE THESIS **77**

LIST OF SYMBOLS

°C	Celsius degree
cm	Centimeter
Da	Dalton
GW	Gigawatt
g	Gram
g/mol	Gram per mol
MHz	Megahertz
µl	Microliter
µm	Micrometer
mg	Milligram
ml	Milliliter
mm/min	Millimeter/ minute
M	Molar
nm	Nanometer
ppm	Parts per million
%	Percent
rpm	Rounds per minute
m^2	Square meters

LIST OF ABBREVIATIONS

ACSS	Acid-Catalyzed Silica Sol
APS	3-aminopropyl trimethoxysilane
AR	Anti-reflective
ATRP	Atom Transfer Radical Polymerization
CRP	Controlled Radical Polymerization
DC	Direct Current
DCM	Dichloro Methane
DLS	Dynamic Light Scattering
DMF	Dimethylformamide
DP	Degree of Polymerization
EtOH	Ethanol
EU	European Union
EVE	Ethyl Vinyl Ether
FE-SEM	Field Emission Scanning Electron Microscope
FTIR	Fourier-Transform Infrared Spectroscopy
GPC	Gel Permeation Chromatography
H_2O	Water
H_3PO_4	Phosphoric Acid
HCl	Hydrochloric Acid
HSNPs	Hollow Sphere Nanoparticles
KOH	Potassium Hydroxide
MgF_2	Magnesium Flouride
$M_{n,GPC}$	Number Average Molecular Weight with GPC
$M_{n,NMR}$	Average Molecular Weight Calculated by ^1H NMR
$M_{n,Theoretical}$	Theoretical Number Average Molecular Weight
$M_{p,GPC}$	Highest Peak Molecular Weight with GPC
MTES	Methyl Triethoxisilane
MTMS	Methyl Trimethoxysilane
$M_{w,GPC}$	Weight Average Molecular Weight with GPC
$M_{z,GPC}$	Z-mean Molecular Weight with GPC
NH_3,NH_4OH	Ammonia
NMR	Nuclear magnetic resonance spectroscopy
PAA	Polyacrylic Acid
PdI	Polydispersity Index
PSD	Particle Size Distribution
PV	Photovoltaic
R	Reflection
RAFT	Reversible-Addition Fragmentation Transfer
RI	Refractive Index
ROMP	Ring Opening Metathesis Polymerization
SEM	Scanning Electron Microscope
SiO_2	Silicon Dioxide
SLAR	Single-Layered Antireflection

TEM	Transmission Electron Microscope
TEOS	Tetraethyl Ortho Silicate
TGA	Thermogravimetric Analysis
THF	Tetrahydrofuran
TLC	Thin Layer Chromatography
TMOS	Tetramethyl Orthosilicate
UV-VIS	Ultraviolet-visible
VTMS	Vinyl trimethoxysilane
γ-MAPTS	γ- Metacryloxypropyl Trimethoxysilane

LIST OF FIGURES

Figure 1.1 Trend in the reduction of the PV module cost..... 2

Figure 1.2 Schematic illustration of HSNPS formation with (A) high mobility PAA aggregates, (B) stable PAA aggregates, (C) highly soluble PAA aggregates, and (D) strong PAA aggregates[8] 5

Figure 1.3 The preparation of SLAR coatings from HSNS infiltrated by ACSS 6

Figure 1.4 TEM images of hollow silica spheres made with different amounts of ammonia: (A) 1.0 ml, (B) 1.5 ml, And (C) 2.0 ml. in all of the samples, the volume of TEOS is 0.50 ml and the quantity of PAA is 0.084 g.. 6

Figure 2.1 SEM images of a cicada wing. (A) large-scale perspective in a top view. (B) cross-sectional view showing the dorsal and ventral surfaces full of nanonipples. (C) higher-magnification cross-sectional view ……..9

Figure 2.2 AR coating illustration 10

Figure 2.3 Layers of a standard PV module..... 11

Figure 3.1 Spin coating process [14]…..……12

Figure 3.2 Dip-coating process..... 14

Figure 4.1 (A) Hydrolysis and condensation rate depending on solution Ph and (B) gel structures obtained depending on solution Ph [30]……17

Figure 4.2 Mechanism of acid- (A) and base-catalyzed (B) hydrolysis reactions [28] 19

Figure 4.3 Mechanism of acid- (A) and base-catalyzed (B) condensation reactions [28] 20

Figure 4.4 The reaction mechanism of one step Stöber process 21

Figure 5.1 Schematic representation of polymerization…… 22

Figure 5.2 Simple classification of polymers 23

Figure 5.3 Types of copolymers 23

Figure 5.4 ROMP reaction 25

Figure 5.5 General mechanism for ROMP polymerization 26

Figure 5.6 Chauvin's mechanism 26

Figure 5.7 Structures of Grubbs generation catalysts 27

Figure 6.1 Sol-Gel preparation process…… 33

Figure 7.1 The reaction mechanism of *endo* norbornene intermediate product …… 35

Figure 7.2 Reaction mechanism of Monomer 1..... 36

Figure 7.3 FTIR spectrum of Monomer 1 37

Figure 7.4 ^{13}C NMR spectrum of hydrolysed Monomer 1 37
Figure 7.5 ^{13}C NMR Spectrum of mixture of Monomer 1 and hydrolysed Monomer 1 38
Figure 7.6 The reaction route of the oxanorbornene monomer..... 39
Figure 7.7 ^{13}C NMR spectrum of Monomer 2 39
Figure 7.8 ^{1}H NMR spectrum of Monomer 2..... 39
Figure 7.9 FTIR spectrum of Monomer 2 40
Figure 7.10 Synthesis route of *exo*-norbornene polymer..... 41
Figure 7.11 ^{13}C NMR spectrum of Poly1-5k..... 41
Figure 7.12 ^{13}H NMR spectrum of Poly1-5k 42
Figure 7.13 ^{13}C NMR spectrum of Poly1-10k..... 42
Figure 7.14 ^{13}H NMR spectrum of Poly1-10k 43
Figure 7.15 FTIR spectrum of Poly1-5k..... 43
Figure 7.16 FTIR spectrum of Poly1-10 k..... 44
Figure 7.17 The hydrolysis reaction mechanism of Poly1-5k & Poly1-10 k 44
Figure 7.18 ^{13}C NMR spectrum of Poly1H-5k..... 45
Figure 7.19 FTIR spectrum of Poly1-5k (red) and Poly1H-5k (turquoise)..... 46
Figure 7.20 FTIR spectrum of Poly1-10k (red) and Poly1H-5k (blue)..... 46
Figure 7.21 Synthesis route of oxanorbornene polymer..... 47
Figure 7.22 ^{13}C NMR spectrum of Poly2-5k..... 47
Figure 7.23 ^{1}H NMR spectrum of Poly2-5k 48
Figure 7.24 FTIR spectrum of Poly2-5k..... 49
Figure 7.25 FTIR spectrum of Poly2-10k..... 49
Figure 7.26 The hydrolysis reaction mechanism of Poly2-5k & Poly2-10 k 50
Figure 7.27 ^{13}C NMR spectrum of Poly2H-5k..... 50
Figure 7.28 FTIR spectrum of Poly2-5k (blue) and Poly2H-5k (red)..... 51
Figure 7.29 FTIR spectrum of Poly2-10k (blue) and Poly2H-10k (red)..... 51
Figure 7.30 Nitrogen TGA graph of the synthesized polymers 54
Figure 7.31 Core-shell formation 55
Figure 7.32 A typical DLS system 1) laser 2) cell 3) detector 4) attenuator 5) correlator 6) computer 56
Figure 7.33 Sol1 5k (red), Sol1 10k (green) post stock solution particle size distribution graph 58

Figure 7.34 Sol2 5k (green), Sol2 10k (red) PolyH in EtOH particle size distribution graph 58

Figure 7.35 Sol2 5k (red), Sol2 10k (green) after TEOS addition particle size distribution graph 58

Figure 7.36 Sol2 5k (red), Sol2 10k (green) post reflux particle size distribution graph..... 59

Figure 7.37 Sol1 5k post reflux particle size distribution graph 59

Figure 7.38 Sol2 5k post reflux particle size distribution graph 60

Figure 7.39 Sol1-5k TEM images a,b: PolyH in EtOH c,d: post stock solution... 61

Figure 7.40 Sol1-10k TEM images a,b: PolyH in EtOH c,d: post stock solution. 61

Figure 7.41 Sol2-5k TEM images a,b: PolyH in EtOH c,d: post stock solution... 62

Figure 7.42 Sol2-10k TEM images a,b: PolyH in EtOH c,d: post stock solution. 63

Figure 7.43 Dip-coater process (left) coated glasses (right) 64

Figure 7.44 Coated glass transmission graph of Sol1-5k-200 and Sol2-5k-200 . 66

Figure 7.45 FE-SEM cross-section images of Sol1-5k-200 67

Figure 7.46 FE-SEM cross-section images of Sol2-5k-200 67

LIST OF TABLES

Table 7.1 Molecular weight distribution 52
Table 7.2 Size distribution of nanoparticles via DLS 57
Table 7.3 %Transmittance and %Haze Measurements of coated glasses..... 64

ABSTRACT

Antireflection Coatings Based On Silica-Polynorbornene Nanocomposites

Olcay İrem İREY

Department of Chemistry

Master of Science Thesis

Supervisor: Prof. Dr. Tarık EREN

Co- supervisor: Dr. Refika BUDAKOĞLU

The interest in sustainable and renewable energy sources is increasing day by day all over the world. The use of photovoltaic modules in this area has become widespread due to the fact that they convert the light from the sun into electrical energy. Anti-reflective (AR) coatings, on the other hand, are being studied with increasing interest due to the fact that they increase the light transmittance of the coated surfaces. The light transmittance reaching the solar cells from the cover glasses used in these modules is around 90% under normal conditions. This ratio can be increased with AR coating onto to the glass surface. It is expected that the mechanical strength of AR coatings will be durable despite the harsh climatic conditions, they will have a long life in atmospheric conditions, the refractive index will decrease and therefore the light transmittance will increase. When the studies are examined, it is seen that the coatings that best meet this condition are the ones in which hollow spherical structures which are used in the sol-gel

formulation. These spherical voids are obtained by decomposing the organic structure inside by tempering the silica nanoparticle templates in sol-gel surrounded by organic internal silica after coating on the glass surface. In the literature, polyacrylic acid (PAA) has been widely used as organic starting material. In this study, carboxylic acid functional polynorbornene-based polymers with two different chain lengths were synthesized by ROMP technique. Structural characterizations of polymers were investigated by GPC, NMR and FTIR techniques. Investigation of particle size in polynorbornene-based sol-gel formulation, the behaviour of these patterns in the sol-gel mechanism, the structure-property relationship and their effect on permeability were investigated by characterization techniques such as TEM, DLS, UV spectrometry, FE-SEM-Side section.

Keywords: Anti-reflective coating, sol-gel, polynorbornene, silica nanoparticle, hollow spheres

ÖZET

Silika-Polinorbornen Nanokompozitlerine Dayalı Yansıma Önleyici Kaplamalar

Olcay İrem İREY

Kimya Bölümü

Yüksek Lisans Tezi

Danışman: Prof. Dr. Tarık EREN

Eş Danışman: Dr. Refika BUDAKOĞLU

Her geçen gün sürdürülebilir ve yenilenebilir enerji kaynaklarına olan ilgi tüm dünyada artmaktadır. Bu alanda foto-voltaik modüllerin kullanımı güneşten gelen ışığı elektrik enerjisine çevirmesi sebebiyle yaygınlaşmıştır. Anti-reflektif (AR) kaplamalar ise, yüzeylerde ışık geçirgenliğini arttırması sebebiyle gün geçtikçe artan bir ilgiyle çalışılmaktadır. Bu modüllerde kullanılan kapak camlarından solar hücrelere ulaşan ışık geçirgenliği normal koşullarda yaklaşık %90 seviyelerindedir. Bu oran, cam yüzeye yapılacak AR kaplama ile arttırılabilmektedir. AR kaplamaların mekanik dayanımının zorlayıcı iklim koşullarına karşın dayanıklı olması, atmosferik koşullarda uzun ömürlü olması, refraktif indeksin düşüp dolayısıyla ışık geçirgenliğinde artış beklenmektedir. Yapılan çalışmalar incelendiğinde bu koşulu en iyi sağlayan özellikte kaplamaların içi boşluklu küresel yapıların sol-jel formülasyonunda kullanıldığı kaplamalar olduğu görülmektedir. Bu küresel boşluklar organik iç yapılı silika ile çevrelenmiş sol-jel içerisinde bulunan silika nano partikül kalıpların cam yüzeye kaplama yapıldıktan sonra temperlenerek içerisindeki organik yapının bozunmasıyla elde

edilir. Literatürde yeralan çalışmalarda poliakrilik asit (PAA) yaygın bir şekilde organik başlangıç malzemesi olarak kullanılmıştır. Bu çalışmada organik yapı için PAA yerine iki farklı zincir uzunluğunda olan polinorbornen esaslı polimerler ROMP tekniği ile sentezlenmiştir. Polimerlerin yapısal karakterizasyonları GPC, NMR ve FTIR teknikleri ile incelenmiştir. Polinorbornen esaslı sol-jel formülasyonunda partikül boyutunun incelenmesi, sol-jel mekanizmasında bu kalıpların davranış şekli, yapı-özellik ilişkisi ve geçirgenliğe etkisi ise TEM, DLS, UV spektrometre, FE-SEM-Yanal Kesit gibi karakterizasyon teknikleri ile incelenmiştir.

Anahtar kelimeler: Anti-reflektif kaplama, sol-jel, polinorbornen, silika nano partikül, içi boş kürecikler

1
INTRODUCTION

1.1 Literature Review

Energy production is an issue that human beings have paid intense attention to for centuries. Easy, fast and excess energy production is the first need that comes to mind in this regard. In the developing and changing world order, the attention to clean, easy, sustainable and renewable energy sources that will be an alternative to the fossil fuel, which is predicted to be depleted in th[e] 21st century, has increased since th[e] 20th century, attracting the attention of scientists and industrial producers. In addition to this, intensive research and collaborations are carried out to become climate-neutral countries by reducing intra - European Union (EU) emissions until 2050, led by developed countries, especially the EU.

Photovoltaic (PV) panels take their place in the field of renewable energy with their developing and improving features every year, by converting the light energy from the sun into electrical energy. The use of solar panels to establish self-sufficient satellites, buildings, factories, cars and even cities on a large scale in terms of energy use all over the world is one of the potential candidates for the realization of these plans. The history of photovoltaic panels is based on earlier dates than we can imagine.

Detection of the first photovoltaic effect in the world was found in 1839 by Alexander Edmond Becquerel, a young 19-year-old French physicist. He realized when electrons were in an excited state in a conduction band, they could move freely through a material, thus creating a current.

1873 The scientist named Willoughby Smith made history as the person who prepared the first photovoltaic assembly in the field of solar panel system by discovering the photoconductivity in selenium. 1877 Scientists named W.G. Adams and R.E. Day found that solids can also create a photovoltaic effect. Then

in 1883, a scientist named Charles Fritts developed the 1% efficient photovoltaic cell. In 1946, more than 60 years later Solar history patented the Russell Ohl modern PV solar panel for the first time in the world [1]–[4].

In the 1950s the world had less than a watt of solar cells powering electrical equipment. In the twenty-first century, after 50 years of continual research and development on silicon and other PV materials, solar panels are now used to power buildings, satellites, and millions of homes all over the world while also producing clean energy. Around 728 GW of solar energy is expected to be installed globally by 2026, when it is expected to reach 1,645 GW. The cost of solar energy has fallen the fastest of all energy technologies. In the 1950s, silicon PV cells cost 76 US dollars per watt, but by 2021, that price had considerably dropped to just 0.20 [5]. From 2000 – 2019 the prices were reduced significantly but the reductions started to level off after that. The figure below shows the trend in the reduction of the cost.

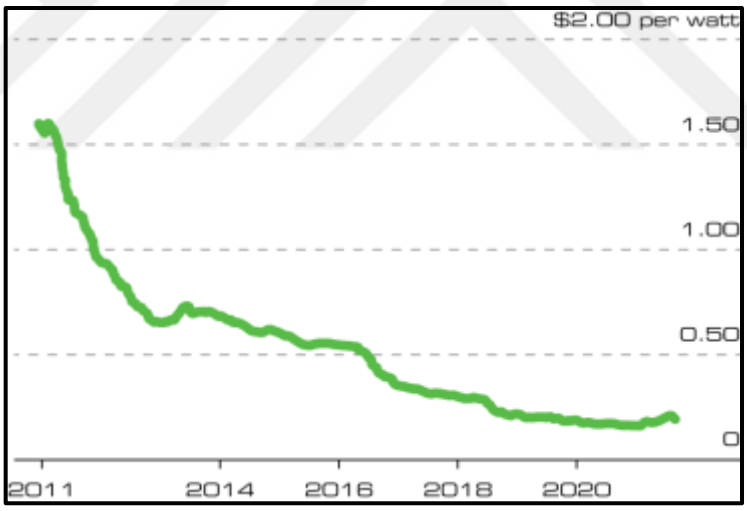

Figure 1.1 Trend in the reduction of the PV module cost

It is important that the glass panels used for the protection of solar cells in photovoltaic modules can provide the maximum contribution to the energy collected by the cells. During the incoming light passing through the glass panels and reaching the solar cells, 8% of the incoming beam is reflected due to the refractive index of the glass (1.55). To prevent this energy loss, the upper surface of the glass used in solar panels is coated with an anti-reflective (AR) coating to

increase the transmittance of the glass. Scientists have also done extensive work on coating glass, one of the oldest materials in history.

AR-coated glasses can be used in optical lenses, architecture, solar panels and many more. To give the glass anti-reflective properties, it is necessary to increase the transmittance by lowering its refractive index. In this direction, forming porous structures in the coating reduces the refractive index, thus increasing the transmittance.

AR coatings can be open pore or closed pore. Being open pore is a term used because there are porous structures on the surface of the coating that meets with air. Since these pores on the surface can interact chemically with organic structures such as water, dirt, etc., it causes a decrease in the mechanical strength of the coating. For this reason, studies in which closed pore thin film coatings are made in such a way that pores are placed in the coating thickness and do not create pores on the coating surface come to the fore. Hollow sphere nanoparticles create the appropriate conditions to obtain a closed pore structure.

1.1.1 Hollow Sphere Nanoparticle

Hollow spheres are a type of special functional material with a large fraction of empty spaces inside, preserved shells and uniform shape. The hollow spheres' density is considerably lower compared to their solid peers of the same size and material because of the hollow core.

Recently, the synthesis of inorganic hollow structures has received a lot of interest because their unique properties, which result from the presence of interior void space, are beneficial for a wide range of industrial and biological applications.

Silica is the most prevalent inorganic matrix, both for mesoporous solid materials and hollow microspheres, due to its well-controlled kinetics for hydrolysis and condensation of silicon alkoxides in aqueous solution, as well as its low density, excellent mechanical and thermal stability, and chemical inertia. Pinnavaia et al. were the first to demonstrate the synthesis of multilamellar mesoporous silica spheres using a vesicular solution of bolaamphiphiles amines [6].

Inorganic hollow spheres are more common, diverse, and stable than polymer shell hollow spheres. The most common coating material is SiO_2 because it has several versatile properties. First and foremost, SiO_2 is hydrophilic and negatively charged, which prevents colloidal sphere aggregation. Second, SiO_2 is adaptable when it comes to porosity, optical transparency, biocompatibility, and mechanical stability.

To create a hollow sphere template, polystyrene and polyacrylic acid (PAA) are widely used as a template in the sol-gel process. In our study, two different polynorbornene derivatives, each with two different molecular weights, were used to form the core of the hollow sphere templates.

PAA is insoluble in ethanol under basic conditions but soluble in water. In ethanol, insoluble PAA-ammonia is used as a template and water is only needed for removing the template. The silica layer is slightly slow to make the PAA template because of the mixture (water, PAA, and ammonia) used. Polyacrylic acid aggregates because of the ammonia in EtOH. The insufficient ammonia makes the carboxylic groups of PAA chains to be weakly aminated and is too little to absorb TEOS hydrolysis and condensation, resulting in silica growth without polyelectrolyte cores. If the ammonia volume is increased further, the PAA-ethanol solution gets less cloudy, and the hollow spheres are greatly condensed [7].

Figure 1.2 demonstrates the relationship between PAA concentration and PAA aggregation. It is suggested that particle size of hollow sphere nanoparticles (HSNPs) become smaller and more monodispersed with a lower PAA concentration [8]. Also using high molecular weight PAA as templates, helps to synthesize ultra-small HSNPs.

As a result, the interaction of PAA and NH_3 was the most crucial factor in controlling the morphologies of the HSNPs.

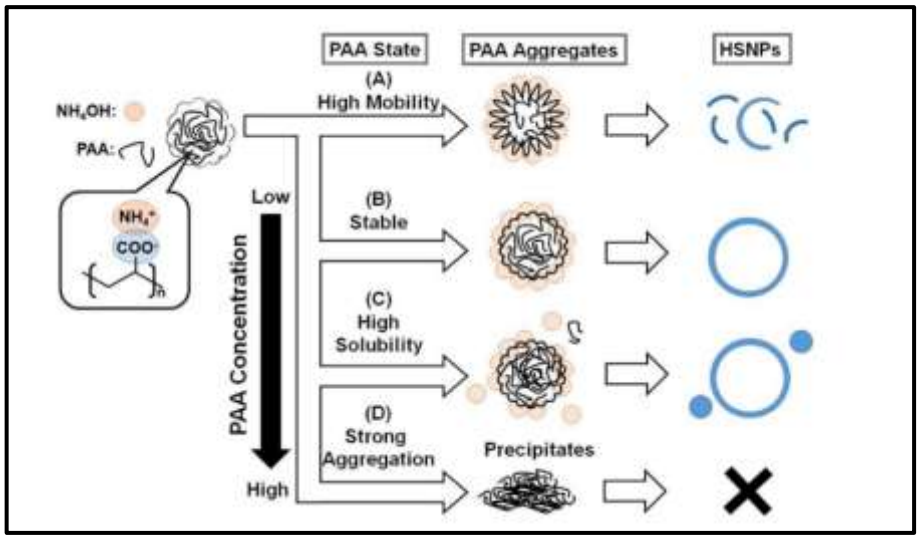

Figure 1.2 Schematic illustration of HSNPS formation with (A) high mobility PAA aggregates, (B) stable PAA aggregates, (C) highly soluble PAA aggregates, and (D) strong PAA aggregates[8]

Depending on the additional processing steps required, this gel can be used to create a variety of materials, including nanoparticles, xerogel, glass, and ceramics. Simple solvent evaporation can be used to create nanoparticles and xerogels. Glassy nature can be induced by melting techniques and the obtained xerogel can be formed as ceramics through heat treatment. As a result, the sol-gel method can be used to produce materials in a variety of shapes and sizes as well as in controlled phases.

The close surface coating was synthesized using silica nanoparticles. The photovoltaic transmissive of anti-reflection thin film and acid-catalyzed sol-gel in hollow silica sphere are both 97.1%. The refractive index ranges between 1.25 and 1.27 [9]. There are lots of studies in this area with different coating methods used. Mostly dip-coating process is used due to ease of application. For instance, dip-coating method is used to create single-layered antireflection (SLAR) coating acid-catalyzed silica sol (ACSS) with a closed-pore structure which is resistant to both moisture and high temperatures, and inexpensive. The photovoltaic transmittance ranges from 96.8% to 97.34% in these coatings. The refractive index ranges from 1.21 to 1.26. It is also resistant to humidity for an extended period of time. Figure 1.3 illustrates the process of creating SLAR coating.[10]

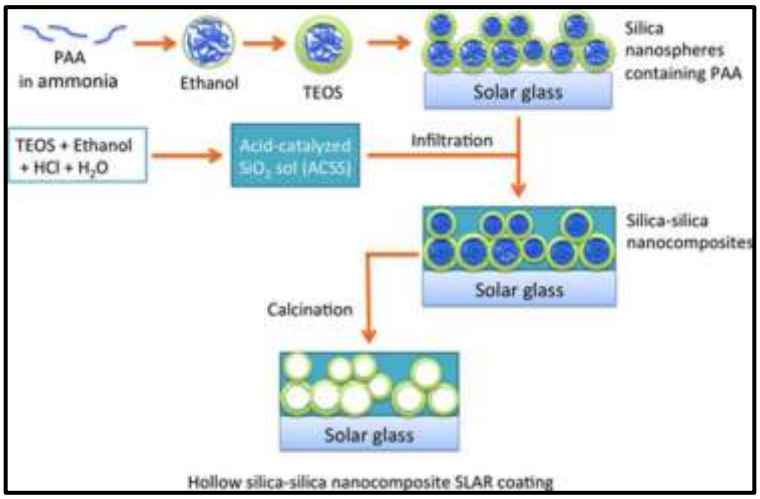

Figure 1.3 The preparation of SLAR coatings from HSNP infiltrated By ACSS

Wan created hollow silica spheres by altering the Stöber process with PAA (polyacrylic acid). They reported that hollow silica spheres with diameters ranging from 25 to 400 nm were synthesized. Their method involves spherical colloid agglutination in an ethanol solution, ammonia hydrolysis of TEOS, and washing to remove the polyelectrolyte. Figure 1.4 illustrates the TEM results obtained with various amounts of PAA [7].

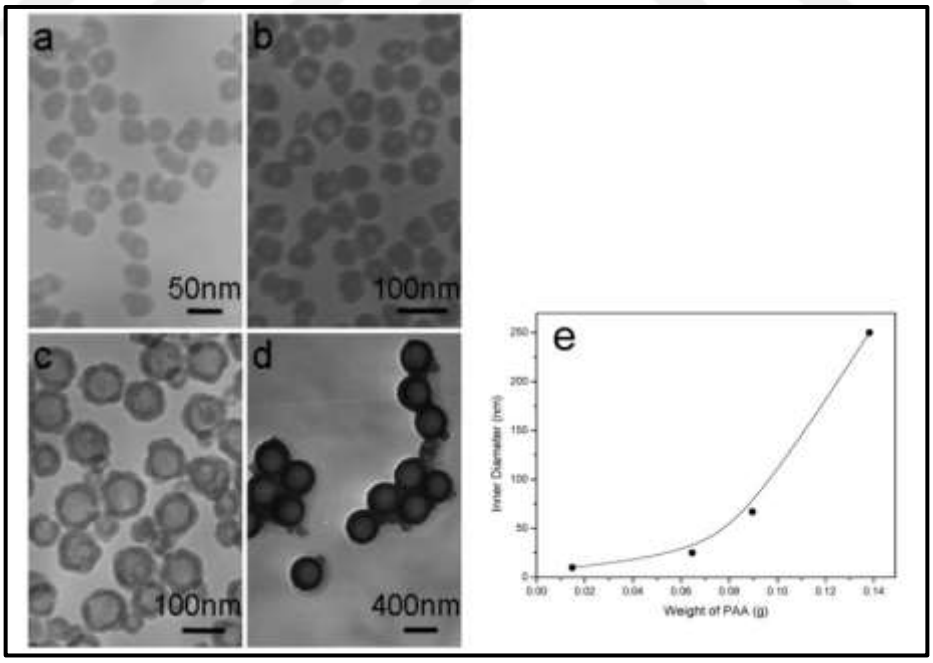

Figure 1.4 TEM images of hollow silica spheres made with different amounts of ammonia: (A) 1.0 ml, (B) 1.5 ml, and (C) 2.0 ml. In all of the samples, the volume of teos is 0.50 ml and the quantity of PAA is 0.084 g.

Buskens et. al, focused his research on the three main coating concepts multilayer interference coatings, graded index coatings, and quarter-wave coatings that reduce reflection at the interface between a transparent substrate and air [11]. These three ideas are introduced, discussed, and then they focus on porous quarter-wave coatings made up of colloidal particles. The optics of multilayer interference coatings can be adjusted for the desired application, and they are mechanically strong and long-lasting. They have been available for several decades, but only for uses where the AR coating adds a significant value. Markets, where the value addition of the AR coating is low to medium, require a low-cost coating that can be applied quickly to large substrates (>1 m^2) in high volumes (multimillion m^2 per year). Because it only has one coating layer, a graded index coating is an example of an AR coating that could be less expensive than a multilayer interference stack. A quarter-wave coating is an illustration of an AR coating that could be less expensive than a multilayer interference stack and does not need surface texturing. Refractive index of 1.23 is necessary for quarter-wave coatings on transparent polymers and float glass, which have a refractive index of roughly 1.5.

It is necessary to introduce pores into coatings to achieve such a low refractive index. In quarter-wave coatings, pores can be introduced in a variety of ways, but the introduction of colloidal particles in particular, hollow spheres and nonspherical particles seems to hold the most appropriate.

1.2 Objective of the Thesis

Polyacrylic acid and polystyrene are widely used polymers to produce core shell structure for the AR coating sol-gel solutions. This study creates an alternative organic source for the core. With the ring opening metathesis polymerization technique, carboxylic acid bearing polynorbornene derivatives with the narrow molecular weight distribution of 5,000 g/mol and 10,000 g/mol are synthesized.

These synthesized polymers with different chain lengths are modified and wrapped with SiO_2. In this way, it is aimed to obtain monodisperse nanoparticles thanks to polymer chains of equal molecular weight used as organic material.

Thus, it is aimed to examine the structure-property relationship of polynorbornenes with different molecular weights in order to form a regular porous structure in anti-reflective coating solutions.

1.3 Hypothesis

Ring opening metathesis polymerization (ROMP) is a versatile technique to investigate structure property relationship. It is a controlled polymerization technique that molecular weight and distribution can be optimized. Here, we produce 5,000 g/mol and 10,000 g/mol carboxylic acid functional polynorbornene series to investigate their hollow sphere particle size effect and distribution. The effect of furan and methylene bridges present in oxanorbornene and norbornene skeleton might be interest for the formation of hollow sphere template and coating performance. When these polymers are used as organic templates, nanoparticles with monodisperse distribution will form in the sol-gel. It is expected that in the resulting coating the SiO_2 shell will form a spherical-shaped, uniformly distributed hollow spheres.

2
ANTI-REFLECTION

One of the most basic optical phenomena is reflection, which happens when light travels across a boundary between two media with different refractive indices. Because of this natural phenomenon, some living things evolved with a physical feature that has anti-reflective surfaces. These AR properties can be seen in the cicada wing, dragonfly wing, moth-eye, and butterfly wing. For instance, the cicada wings' hexagonally close-packed protrusions have both an anti-reflection and an anti-wetting function. SEM images of cicada wing is shown in Figure 2.1. Inspired by these creatures, scientists developed the physical and chemical conditions necessary to give AR properties to material surfaces [12], [13].

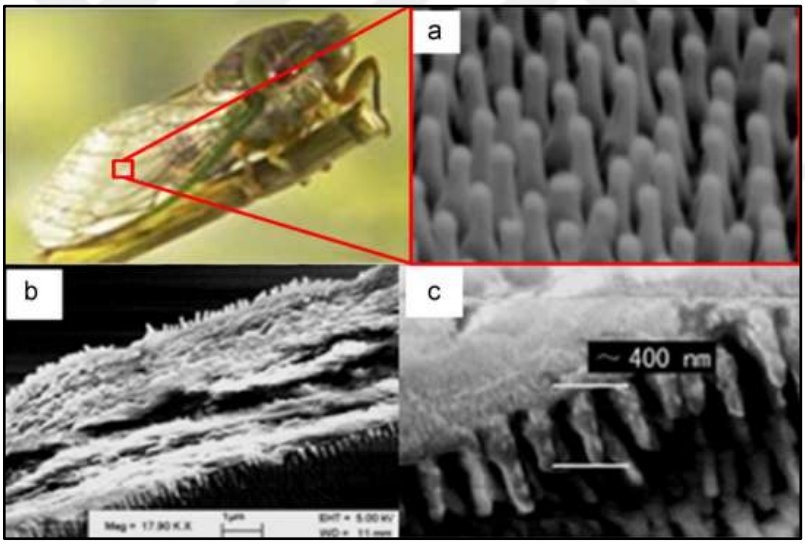

Figure 2.1 SEM images of a cicada wing. (A) large-scale perspective in a top view. (B) cross-sectional view showing the dorsal and ventral surfaces full of nanonipples. (C) higher-magnification cross-sectional view.

2.1 What is Anti-reflection

Reflection is the phenomenon of waves hitting a reflective surface in a homogeneous medium, changing direction, and returning to the medium from which they came. Reflection is an undesirable situation, especially in areas where

the incoming light needs to be collected at the maximum level. Optical anti-reflection, which is utilized in many applications including solar cells, diodes, optical and optoelectronic devices, displays, sensors, anti-glare glasses, and more, refers to the process of minimizing reflection. For example, PV solar panels require a minimum level of reflection of the incoming light. By applying an antireflective coating on the glass surface, the reflection can be minimized. AR Coatings can significantly improve light transmission. The fundamental mathematical model for the reflection of coatings is provided by the Fresnel equation [14]. Refractive index (RI) is the major parameter for characterizing the transmission of light in the medium. AR coatings have lower RI values compared to bare glass and it helps to maximize the transmission of light [15]. Visible light travels from air ($n_0 \approx 1.0$) into the glass ($n_S \approx 1.5$), and the value of Reflection (R) is 4% on a single reflection. (Figure 2.2) Therefore 96% of the light actually enters the glass, and the rest is reflected from the surface. To reduce this loss, antireflective coatings can be applied to the glass surface. This thin film coating must have a thickness of one-quarter of the wavelength of light ($\lambda/4$) and its RI must be 1.22 according to the Fresnel equations. But with the natural materials, the RI can only be reduced to 1.38 using MgF_2. To reduce the refractive index and reach to this calculated value of RI, Yoldas et al. suggested creating hollow structures within the coating [16].

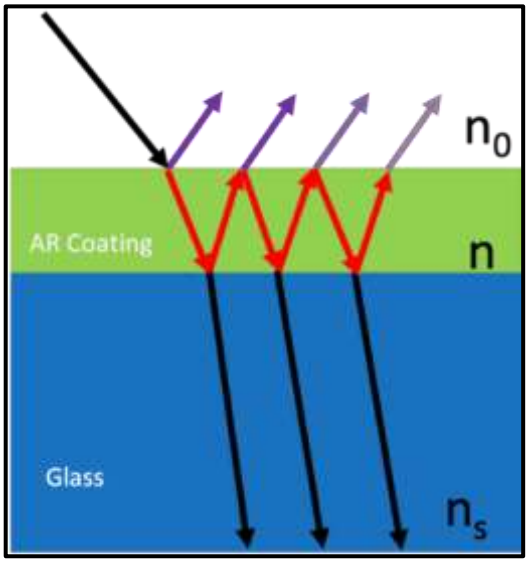

Figure 2.2 AR coating illustration

2.2 PV Module with AR-Coated Glass

The use of solar panels, one of the renewable energy sources, is increasing. Photovoltaic modules, which can be positioned on the roofs of houses, factories, and large lands, have great importance as they provide green energy production. Sunlight is used by solar panels to collect radiant energy, which is then transformed into direct current (DC) power. Glass surfaces are used to allow light to reach the solar cells and to protect them from climate and environmental conditions. The use of AR-coated glasses in PV modules is preferred because the light transmittance of flat glass is 1.50, and therefore only 96% of light can travel through the glass surface and reach solar cells. AR-coated glass can be produced by many different methods. Although coatings made by roller or spray are preferred on an industrial scale, dip coating on a laboratory scale is a very efficient method which will be discussed later. Figure 2.3 shows the layers of a standard PV module below.

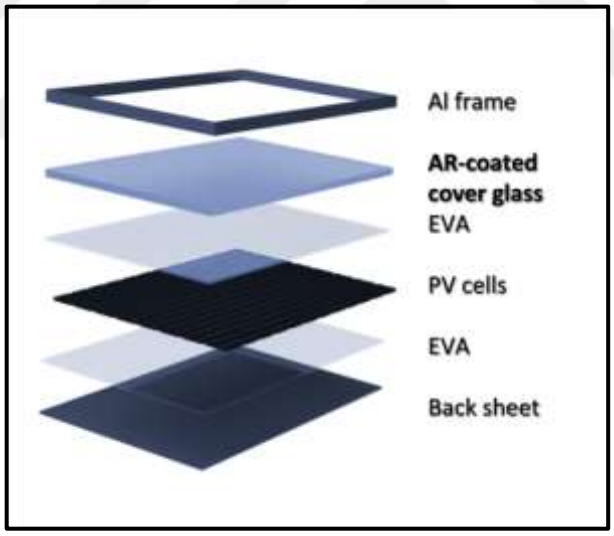

Figure 2.3 Layers of a standard PV module

3
SOL-GEL COATING METHODS

The wet chemical sol-gel processing has versatility for liquid film deposition on different kind of surfaces, especially on the glass. It provides convenience with different coating applications such as spray coating, spin coating and dip-coating. Each of these techniques has a unique ease of application according to the needs of the coating. Sol-gel approach offers several advantages inherent to the technique, including the possibility to coat large, curved substrates using these simple deposition techniques and the ability to obtain homogenous coatings, as well as coatings with tailored inhomogeneity. Dip coating is the most popular deposition technique, especially for laboratory applications. Its popularity is largely due to its straightforward processing, low cost, and high coating quality. However, other methods like spin coating or spray coating are also useful in specific situations. The most common application methods for sol-gel coatings are described below [17], [18].

3.1 Spin Coating

Spin Coating entails depositing a small amount of viscous film material and then rotating the substrate fast (for example, at 3000 rpm), which causes the droplets to expand due to centripetal force. Figure 3.1 illustrates the spin coating process.

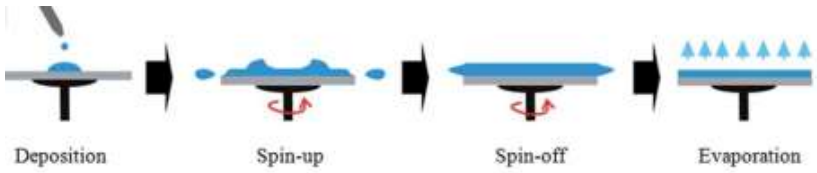

Figure 3.1 Spin coating process [14]

3.2 Spray Coating

Spray-coating is quite a facile method, which is not specific to a particular substrate and can be easily applied to a large surface area. As spray-coating does not typically require other complicated and costly processes, it is commercially feasible for a wide range of applications. This method is simple, fast, material efficient, easy to use, carried out in a non-vacuum system and permits to obtain films with required properties for large-area applications [15].

3.3 Dip-Coating

In this process, the substrate is dipped and withdrawn from the desired solution at a controlled rate. When a substrate is withdrawn from a liquid coating sol, a wet liquid thin film is deposited on the surface. A subsequent curing or sintering procedure (post-treatment) is then required to produce the coated material. Dip coating is a simple, flexible, and cost-efficient coating technique that in combination with sol-gel processing allows the application of a variety of oxide and inorganic-organic hybrid materials on both large area and complex-shaped substrates. It is a well-established industrial coating technique with a long-standing tradition in the deposition of large-scale antireflection coatings and speciality interference filters.

In the dip-coater, it is possible to control the final properties such as the thickness of the coating by varying the withdrawal speed. There is an inverse proportionality between the withdrawing speed and the coating thickness. This is because if the coated surface is pulled slowly, the wet liquid film physically attached to the surface flows down due to gravity and the solution's own viscosity, leaving a thin layer of coating behind. There is not only one optimum withdrawal speed. It changes with the coating sol density stability and viscosity [14], [17]. Figure 3.2 illustrates the dip-coating process briefly.

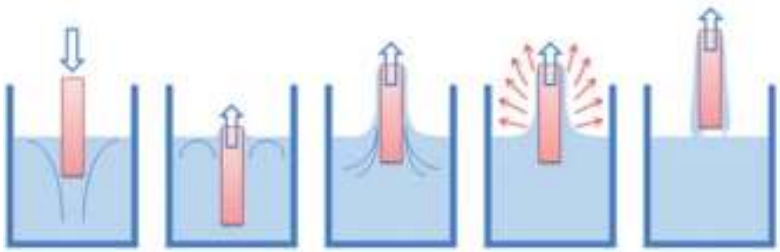

Figure 3.2 Dip-coating process

4
SOL-GEL METHOD

The invention of the sol-gel technique dates to 1846, when Ebelman noticed that tetraethoxysilane slowly hydrolyzed with ambient moisture to form gel. But it was much later that scientists started to pay special attention to this topic [13].

After Kistler's work on aerogels in 1931 [19], [20], studies on metal alkoxide mixtures and thin-film coatings were carried out by several scientists, but it did not attract much attention in material science [21]–[23]. Dislich's work on new routes to multicomponent oxide glasses in 1971 helped realize the potential in this field and research started to gain momentum [24]. In addition, Stöber worked on the mechanisms of controlled growing silica nanoparticles during this period. This study examined the hydrolysis and condensation reactions of TEOS, drawing attention to its role in the sol-gel formation mechanism. Today, the complex and rapid sol-gel mechanism is still being studied based on this study [25]

The ability of nano-sized particles (~1-1000 nm) to remain in the colloid as a suspension dominated by only van der Waals and surface charges without being affected by the gravitational force is defined as "sol". All particles in the sol make a random type of motion called Brownian motion this helps the particles to remain hovering in the medium [17], [26]. According to the strength of the solvent-particle interactions, sols can be classified as either lyophilic or lyophobic (strong solvent-particle interaction). A “gel” is a solid that has liquid in it. It is made out of a network structure where liquid and solid combine easily. Not every sol can be transformed into a gel. An essential need for gel formation is a strong solvent-particle interaction [27].

4.1 Advantages and Disadvantages of Sol-gel Method

Sol-gel is a very advantageous method compared to the classical melt quenching method in obtaining homogeneous and high-purity nanoparticles at low

temperatures while the chemical conditions are mild. It has a very flexible route that particle size and particle surface modification can be done according to the needs of the end product. Metal alkoxide initiators are generally volatile and can be easily purified, making it easier to obtain a high-purity final product. The size of the porous structures and the ability to modify their shape provide variety in the production of functional materials such as antireflective or optical coatings.

However, the sol-gel method has some disadvantages. The sensitivity of the obtained coating solution to moisture creates a stability problem. The shelf life of the solution may also be short accordingly. The formation of stress cracks during the calcination of the coated glass material, the shrinking of the pores and reproducibility are the limiting features of this method for large-scale production plants to specialised applications, but they are not unsolvable. The aforementioned problems can be minimized by controlling the aging and calcination steps carefully [18].

4.2 Critical Parameters of Sol-Gel

4.2.1 Precursors

Precursors used in the sol-gel process must be soluble in the reaction medium. It can be divided into two main categories according to the nature of the precursor, these are inorganic precursor (chlorides, nitrates, sulfides, etc.) and alkoxide precursor. The most commonly used alkoxysilane precursors are as follows:

- Tetraethyl orthosilicate (TEOS)
- Tetramethyl orthosilicate (TMOS),
- Methyl triethoxisilane (MTES)
- Methyl trimethoxysilane (MTMS)
- Vinyl trimethoxysilane (VTMS)
- 3-aminopropyl trimethoxysilane (APS)
- γ-metacryloxypropyl trimethoxysilane (γ-MAPTS)

The types and concentrations of silicon alkoxides have an impact on the rates of condensation and hydrolysis. The viscosity of the solution increases as the precursor concentration increases.

The size of the alkoxy groups in the structure of the precursor used adversely affects the reaction rate. Large alkoxy groups create steric hindrance and crowd the transition state. Tetramethoxy silane (TMOS) hydrolyzes quicker than tetraethoxysilane (TEOS) because of its less crowded alkoxy groups. By using TEOS, the reaction time and thus the controlled formation of the particles can be provided [18], [28], [29].

4.2.2 pH/Catalysts

In cases where the precursor used is a silica alkoxide derivative ($Si(OR)_4$), the pH varying according to the catalyst chosen is informative about whether there will be a hydrolysis or condensation reaction in the medium. Although alkoxy silanes and water typically react slowly, the reaction can be sped up by using acid or base catalysts [29]. In acid-catalyzed sol-gel media, the hydrolysis reaction rate is higher than condensation, resulting in weakly cross-linked polymeric structures. In reactions under basic ambient conditions, more branched clusters are formed as a result of rapid hydrolysis and condensation of alkoxy silanes [28]. Figure 4.1 shows the gel structures created by the hydrolysis and condensation reaction rates, which vary based on the solution's pH.

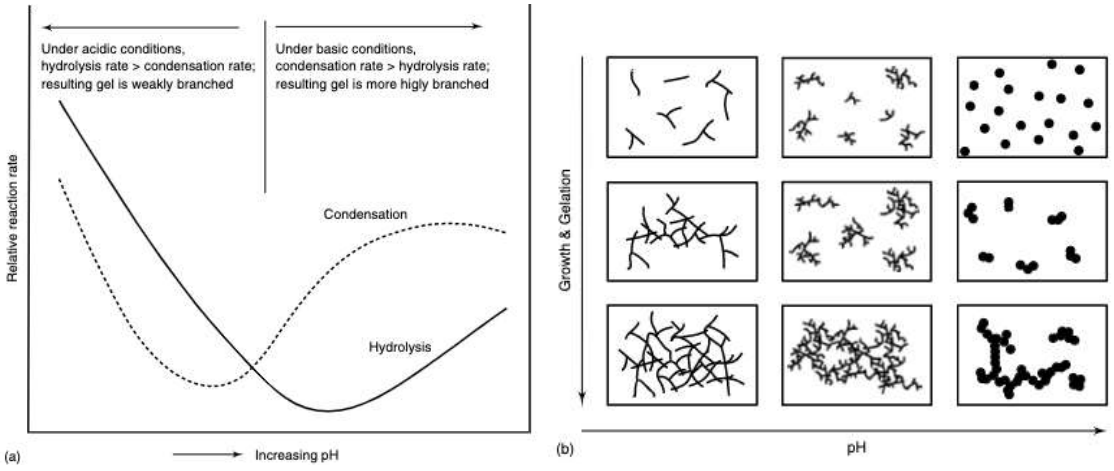

Figure 4.1 (A) Hydrolysis and Condensation Rate Depending on Solution pH and (B) Gel Structures Obtained Depending on Solution pH [30]

Due to the lower electropositivity of Si, TEOS is known to be less prone to hydrolysis than transition metal alkoxides. To create a stable environment in sol, changing the pH from the isoelectric point is necessary (the isoelectric point of silica is pH 2.2). Because of the reduced particle-to-particle interaction caused by the surface charges, neither aggregation nor agglomeration occurs. The particle-to-particle distance can be decreased with pH change or solvent evaporation. if so, the surface charges decrease and the probability of gelation increases. Thus, any solvent vaporization must be done quite carefully. Further strong particle-to-particle interactions results with irreversible agglomeration [29].

4.2.3 The H_2O/Alkoxy Molar Ratio

The mole ratio of H_2O/alkoxy (R) also affects the rate of hydrolysis and condensation reactions. The most suitable water and alkoxy ratios should be determined to control both the reaction rate and gelation time and the structure of the product obtained [18], [29]. For complete hydrolysis, the stoichiometric ratio of water to alkoxide is 4:

$$Si(OEt)_4 + 4H_2O \leftrightarrow Si(OH)_4 + 4EtOH$$

To obtain SiO_2 thin film coatings, R=2 is insufficient for complete hydrolysis and accordingly, higher R values are required [31]. Also, at R values less than 2, a matrix with a more open structure due to incomplete hydrolysis, and consequently less crosslinking in the sol-gel material [32].

4.2.4 Temperature

Temperature is a critical factor at every stage of the sol-gel process. In cases where the reaction ambient temperature is increased above the boiling point of the solvent used, the solvent will evaporate, and this will pave the way for gelling or undesired precipitation. The film thickness is also directly affected by temperature because it changes the solution's viscosity during the coating process. The part where the temperature parameter is most effective on the sol-gel is the calcination of the coated glass. Since the Si-O-Si covalent bonds formed because of hydrolysis

and condensation reactions are not stable under 450 °C, the calcination temperature can be between 450-1000 °C [29], [33], [34].

4.3 Reaction Mechanism

In silica sol-gels, the reaction mechanism, the amount of silica used and the crowded R groups it contains, whether the catalyst is acid or base, and accordingly the pH, the amount of solvent and water play a significant role during hydrolysis and condensation reactions. Figure 4.2 and 4.3 shows the reaction mechanism of hydrolysis and condensation reactions of acid and base catalysts.

Hydrolysis: $Si–(OR)_4 + H_2O \leftrightarrow Si–(OR)_3(OH) + ROH$

Condensation: $(OR)_3–Si\text{-}OH + HO–Si–(OR)_3 \leftrightarrow [(OR)_3Si–O–Si(OR)_3] + H–O–H$

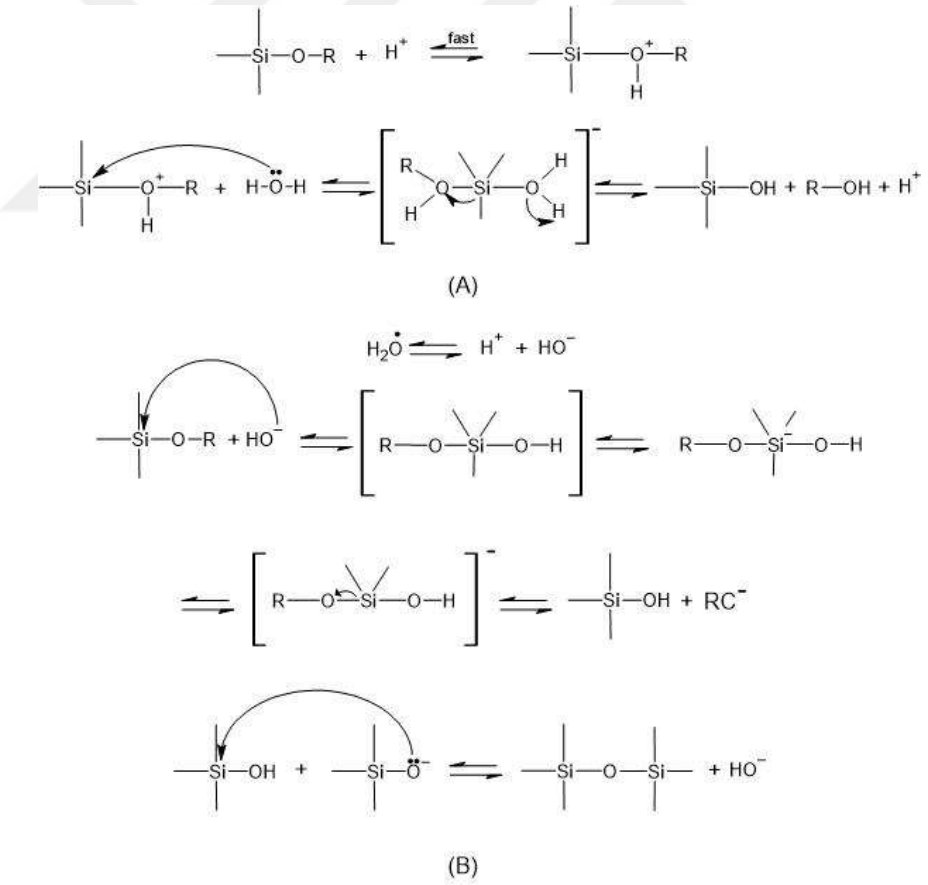

Figure 4.2 Mechanism of acid- (A) and base-catalyzed (B) hydrolysis reactions [28]

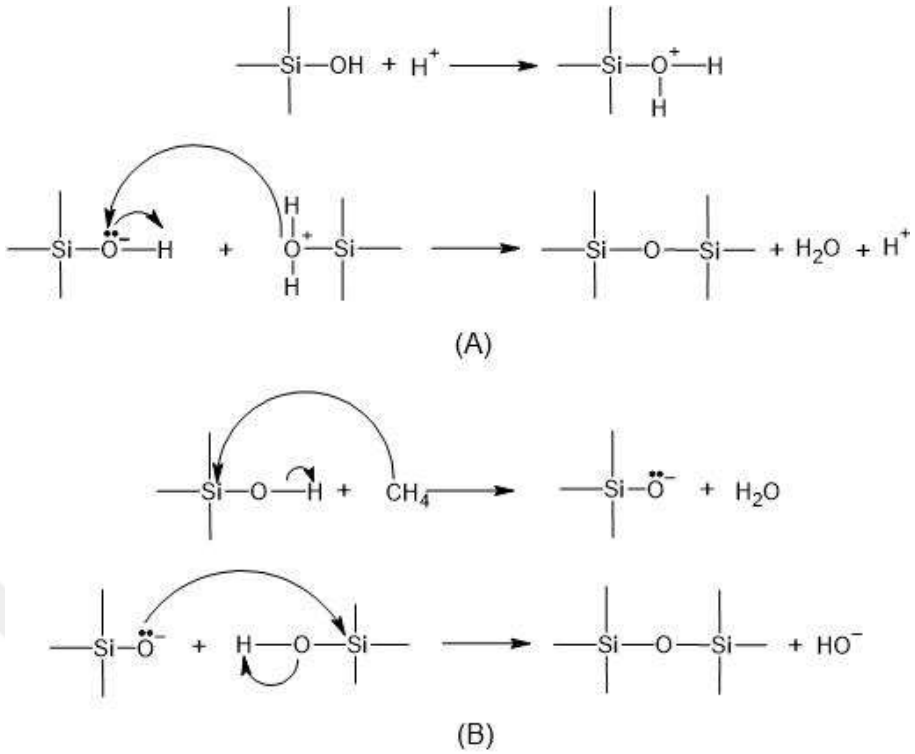

Figure 4.3 Mechanism of acid- (A) and base-catalyzed (B) condensation reactions [28]

4.4 Stöber Process

In 1968, Stöber et al. [35] produced controlled silica nanoparticles with diameters of 500 nm-2 μm using TEOS, ammonia as catalyst, ethanol and water as solvent and elucidated its mechanism. The narrow size distribution of the silica particles could be regulated by varying the temperature, reactant composition, and solution pH. One step Stöber process model includes both hydrolysis and the condensation of TEOS at the same time. Figure 4.4 illustrates the reaction mechanism of one step Stöber process.

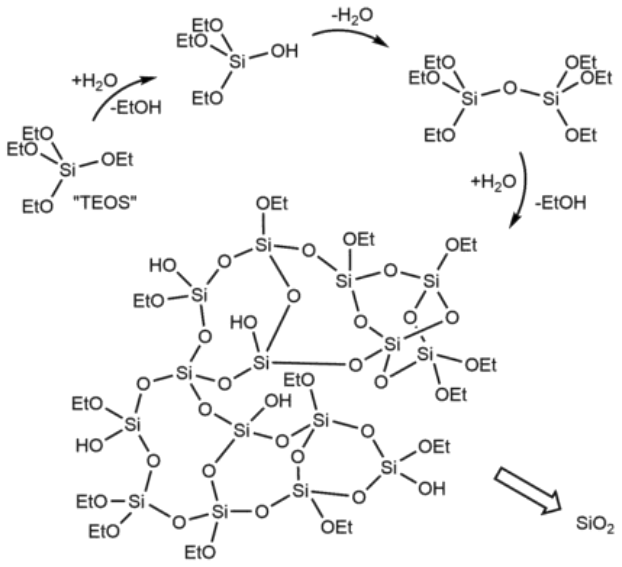

Figure 4.4 The reaction mechanism of one step Stöber process [36]

The Stöber synthesis has the advantage of having the ability to transfer the nanoparticles into aqueous solutions with ease and being readily scaled up for commercial purposes. Even after 50 years, monodisperse silica nanoparticle production is still being studied in the light of this method. According to Bogush, the primary factors that affect particle size and distribution are reaction temperature, water, solvent type, and ammonia concentration. Additionally, it was discovered that the sol-gel process was significantly reliant on the reactant mixing modes and drying technique [28], [37], [38].

5
POLYMERS

A polymer is a macromolecule consisting of many small molecules connected by covalent bonds. As shown in Figure 5.1, under suitable conditions small molecules called monomers make chemical bonds with each other as a result of the polymerization reaction and turn into polymer molecules [39].

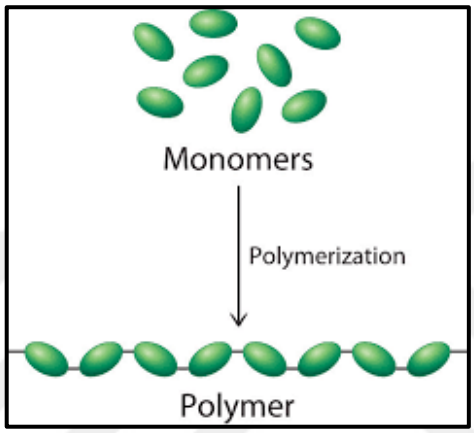

Figure 5.1 Schematic representation of polymerization

The size of their molecules is the key characteristic that sets polymers apart from other classical chemical compounds. Therefore, everything with a large molecular weight may be referred to as a polymer. Macromolecular structures provide a significant contribution to polymers' outstanding characteristics. For instance, above a given chain size, the necessary mechanical characteristics are achieved. The properties of a polymer are influenced by its chain form.

Polymers can be categorized in two as homopolymers and copolymers depending on how many different monomers it contains. a As it shown in Figure 5.2 if the polymer consists of the repetition of a single monomer unit, it is called a "homopolymer". In contrast, "copolymers" are composed of at least two distinct types of monomer subunits that are joined together.

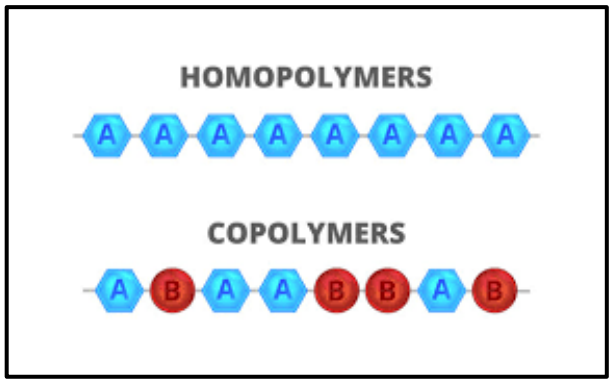

Figure 5.2 Simple classification of polymers

Depending on the arrangement of the monomer subunits, copolymers can be divided into block, random, and alternative types as shown in Figure 5.3. While random polymers are created by the random connecting of monomer subunits, blocked polymers are created by joining two larger chains. The third kind, alternate copolymers, are created by alternatively joining the monomer subunits [40].

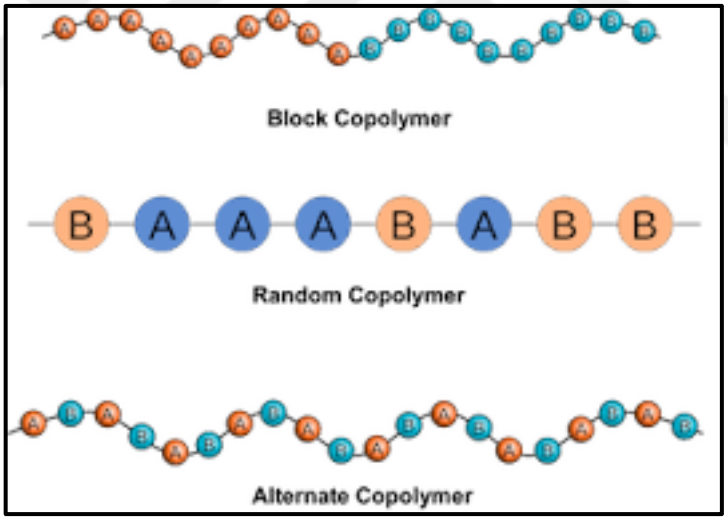

Figure 5.3 Types of copolymers

Polymer synthesis can be categorized into two groups: chain-growth polymerization and step-growth polymerization. In step-growth polymerization, the molecular weight of the polymer steadily rises. High molecular weight macromolecules are produced as a result of the polymer chain's continued growth because monomers are creating dimers and dimers are forming trimers. Step growth polymerization is more costly than chain-growth polymerization because

it requires higher pressure and temperature. Thus, the chain-growth process is used to produce a lot of synthetic polymers [41], [42].

5.1 Controlled Polymerization

The utilization of polymers is significantly influenced by their mechanical characteristics. Various processing and synthesis techniques affect the mechanical characteristics of polymers. A living/controlled polymerization process without a chain transfer or termination step was first described by Swarzc in 1956 [42]. The controlled polymerization approach allows for both the advance specification of the polymerization degree and the production of polymers with a defined range of molecular weight. Furthermore, employing the controlled polymerization technique results in the production of monodisperse polymers with uniform chain lengths [42], [43].

Synthesis of polymers with chosen molecular weights is possible thanks to the controllable polymerization method, which guarantees that the reaction will continue until all the monomers present in the reaction medium have been consumed. Some important examples of controlled/living polymerization are "Controlled Radical Polymerization" (CRP), "Reversible-Addition Fragmentation Transfer" (RAFT), "Atom Transfer Radical Polymerization" (ATRP), nitroxide-mediated polymerizations, and “Ring-Opening Metathesis Polymerization” (ROMP) [44] .

5.2 Ring-Opening Metathesis Polymerization (ROMP)

Olefin metathesis polymerization allows the synthesis of polymers containing double bonds by leaving a monomer containing double bonds. Acyclic diene metathesis polymerization (simple olefin metathesis polymerization) and ring-opening metathesis polymerization are the two classes that olefin metathesis polymerization is investigated.

The ring-opening reactions that transform cyclic monomers into linear polymers with desired molecular weight is called ring-opening metathesis polymerization (ROMP). The carbon-carbon double bonds are protected during the

polymerization process (Figure 5.4), which makes the ROMP technique significant [45], [46]. Numerous cyclic monomers can be polymerized by ROMP, including lactones, lactams, alkenes, and cyclic olefins such as norbornenes. Cyclic olefin derivatives are the most widely used monomer for ROMP because their high level of ring strain allows for quick polymerization. It is possible to produce a variety of polymer structures more precisely with narrow molecular weight distributions since the polymerization is controlled depending on the choice of an appropriate initiator and monomer in ROMP technique [47]. A special metal-mediated carbon-carbon double bond excess technique based on olefin metathesis serves as the mechanism for ROMP polymerization [48]. While a polymer is building via ROMP, the unsaturation associated with the monomer is preserved. This conservation is a key aspect of ROMP that sets it apart from more conventional olefin addition polymerizations.

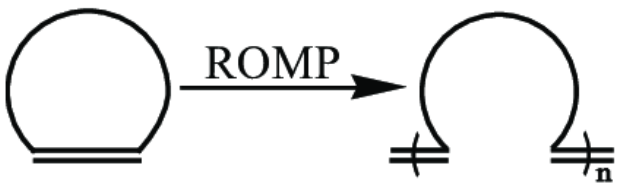

Figure 5.4 ROMP reaction

The overall ROMP mechanism according to Chauvin's concept is shown in Figure 5.5. A cyclic olefin is coordinated with a transition metal alkylidene complex to begin the initiation process. The metallacyclobutane intermediate, which has four members and serves as the start of a continuous polymer chain, is produced by the [2+2] cycloaddition. Then, a new metal alkylidene is created by the cycloreversion reaction of this intermediate. The incorporation of the monomer maintains that, despite the end compound's size increase, its reactivity to cyclic olefins remains identical to that of the initiator. During the propagation stage, the polymerization is maintained by repeating comparable steps up until 100% monomer conversion is accomplished, the reaction reaches equilibrium, or the process is terminated.

Most typically, ROMPs are artificially ended by introducing a particular reagent. This reagent performs two tasks: it shifts the metal group with a recognized functional group and selectively removes and deactivates the transition metal from the developing polymer chain's end [39]. Typically, ethyl vinyl ether can be used to change transition metal from the end of the polymer chain with carbon functional group as phenyl and alkene.

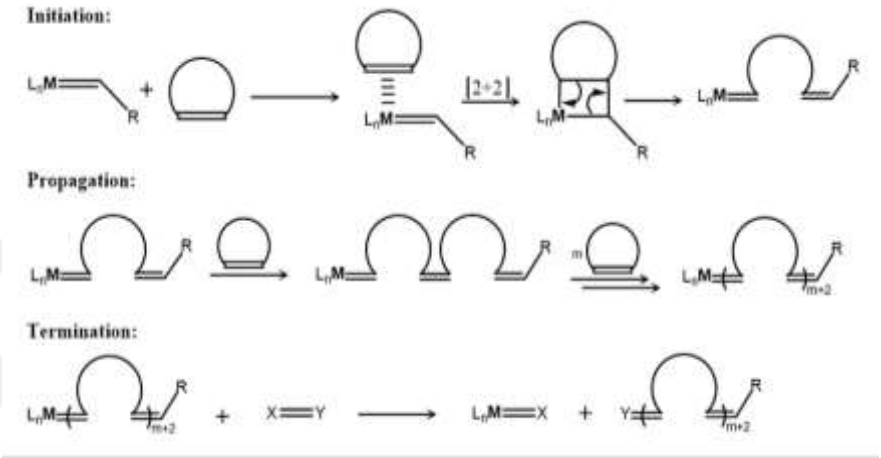

Figure 5.5 General mechanism for ROMP polymerization

In a nutshell, it can be stated that because ROMP is a well-controlled process, it yields the desired molecular weights, uniformity of chain lengths, and balance of hydrophobic/hydrophilic groups in the synthesis of the polymers.

Chauvin demonstrated that a metal complex is necessary for the formation of a metathesis reaction using a specific metathesis mechanism. (Figure 5.6)

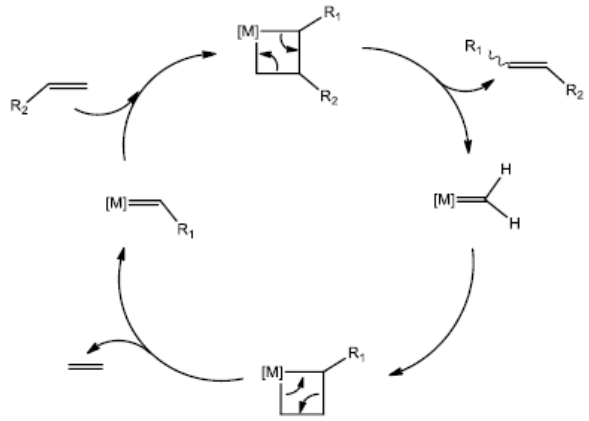

Figure 5.6 Chauvin's mechanism

Transition-metal-based metathesis catalysts such as tungsten, titanium, molybdenum, or ruthenium are used in ROMP. Functional group tolerance is one of the important desired properties for the catalyst. For the monomers including olefin functional groups, reactivity increases when ruthenium-based catalysts are used. Transition metal complexes based on ruthenium are used in the polymerization of cyclic olefins such as norbornenes [49]. Figure 5.7 shows structures of the Grubbs generation catalysts.

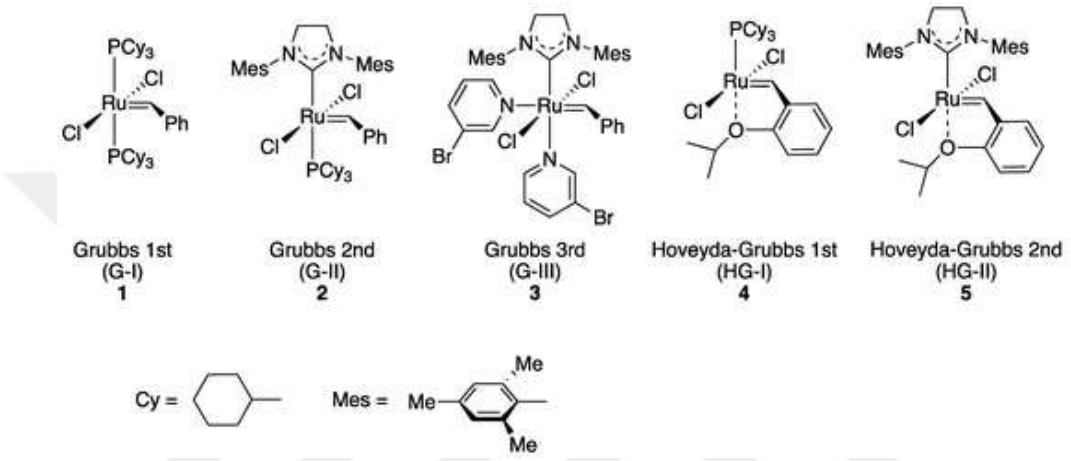

Figure 5.7 Structures of Grubbs generation catalysts

6
EXPERIMENTAL

6.1 Materials & Methods

6.1.1 Used Chemicals

Dicyclopentadiene, furan, maleic anhydride, chloroform, methanol, and toluene are used in monomer synthesis. Diethyl ether, EVE %30 in DCM, DMF and Grubbs 3rd generation catalyst (obtained from Grubbs 2nd generation) is used without further purification in the process of polymerizations and purchased from Sigma Aldrich. Tetraethyl orthosilicate %99 (TEOS), NH_4OH %28, Hydrochloric acid %37, Ethanol %99 Absolute is also used without further purification and purchased from Sigma Aldrich to produce sol-gels.

6.1.2 Used Equipment and Devices

Characterization involved FT-IR spectroscopy (Perkin-Elmer, FT-IR), ^{1}H (500 MHz), ^{13}C (75 MHz) NMR spectroscopy (Bruker-500 MHz), Transmission Electron Microscope TEM (Hitachi HighTech HT7700), Field Emission Scanning Electron Microscope (Hitachi High-Tech FE-SEM Regulus8220), UV-VIS spectrometer (Perkin-Elmer Lambda 950), Transparency and haze meter (BYK haze-gard i), Dynamic Light Scattering (ZetaSizer Nano ZS), Dip Coater (KSV NIMA Dip Coater, Single Vessel Medium), Oven (Carbolite PN200), Muffle furnace (Lenton).

6.2 Method

In this study, it was investigated whether sol-gels prepared using synthesized polymers form an anti-reflective structure when the glass surface is coated. The purity of monomer synthesis is controlled by TLC, polymer synthesis is characterized by NMR and GPC, and prepared polymers are dissolved in ammonia and characterized with FTIR and NMR. The coating solution is obtained by following the particle size and pH along the sol-gel synthesis route. Then the solution is aged. Nanoparticles are examined by TEM analysis from the aged sol.

With this sol, the coating is made on one surface of the glasses, curing and tempering processes are carried out. Transmittance and SEM cross-section examinations of the coated glasses are performed. In addition, TGA analysis of polymers is made. In this way, experimental sets with outstanding features from coated glasses are detected then all results are evaluated together.

6.3 Synthesis of Monomers

6.3.1 Synthesis of (1R,2S,6R,7R)-4-oxatricyclo [5.2.1.$0^{2,6}$] dec-8-ene-3,5-dione

Dicyclopentadiene has been cracked at 170 ºC and distilled to a flask that it cooled and kept 0ºC to collect cyclopentadiene [50]. In another flask freshly distilled 9.4 ml (0.114 mol) cyclopentadiene (66.103 g/mol) was added to 10.2 g (0.104 mol) maleic anhydride 98.06 g/mol) in 180 ml of chloroform at 0 ºC. The reaction was stirred at room temperature in the dark for 5 hours. Chloroform was evaporated with a rotary. Recrystallization was done with 2-3 ml of boiling methanol. It was added to dissolve all the crystals and stirred for a while to get the solution to room temperature. This process was repeated 2 times until no more crystal residue remained in the solution when temperature dropped to 25 °C. The next day the crystals were washed with cold methanol and recrystallized once more then dried in an oven. Purity of the crystals were analysed with TLC (5 Hexane: 1 Ethyl acetate) to check impurities and residual *endo* if present or not ($R_{f,\ Endo}$ =0.23 and $R_{f,\ Exo}$=0.34). The yield was 50%.

6.3.2 Synthesis of (2R,6S)-4-oxatricyclo [5.2.1.$0^{2,6}$] dec-8-ene-3,5-dione (Monomer 1)

5.4065 g (0.033 mol) of (1R,2S,6R,7R)-4-oxatricyclo [5.2.1.02,6] dec-8-ene-3,5-dione (164.16 g/mol) was kept in a 50 ml round bottom flask using a Vigreux column under Nitrogen atmosphere at 200 °C for 2 hours since the melting point of the monomer is 164 to 167 °C. Then the temperature was lowered to 120°C and 5.40 ml of toluene was added carefully via syringe. The supernatant was discarded, and the precipitated crystals were kept at room temperature. To that solution, 2-3 ml of boiling toluene was added to dissolve all the crystals and stirred for a while to get the solution to room temperature. This process was repeated 2

times until no more crystal residue remained in the solution when the temperature dropped to 25 °C. The recrystallization process was completed by keeping it in the freezer overnight. Then, obtained crystals were washed with cold toluene, filtered, and dried in a vacuum oven, impurities controlled by TLC whether the *endo* adduct remains or not. The yield was 23.6%

6.3.3 Synthesis of Furan Maleic Anhydride Diels Alder Product (4,10-Dioxa-tricyclo [5.2.1.$0^{2,6}$] dec-8-ene-3,5-dione) (Monomer 2)

10 grams (0.102 mol) maleic anhydride (98.06 g/mol) was dissolved in flask with 200 mL THF. 33 mL of furan was added to the flask and add nitrogen to the medium for 5 minutes. Since the product is sensitive to light, the flask is wrapped in aluminium foil and the dark room is allowed to react for 4 days. After 4 days, crystalline product is obtained. Washing for purification; It is made by filtering with 200 mL cold THF (100 mL × 2) from the trumpet and dried in a vacuum oven. Pure white crystal obtained. The yield was 78%

6.3.4 Synthesis of Grubbs 3rd Generation Catalyst

Grubbs 3rd generation catalyst is synthesized from Grubbs 2nd generation catalyst. 0.2 g Grubbs 2nd generation was placed in a septum capped vial and 0.5 mL of 3-bromopyridine was added and mixed under N_2 for 10 minutes. After that, it was precipitated and washed with pentane. Then dried with nitrogen and wrapped in aluminium foil to prevent it from being affected by light and stored in the refrigerator at +4°C. (M_W of Grubbs 3rd generation catalyst: 884.48 g/mol).

6.4 Polymerizations of Norbornene Monomers with ROMP

A total of four different polymers were synthesized from the above-mentioned monomer 1 and monomer 2 with a molecular weight of 5000 and 10000 g/mol. The amount of Grubbs catalyst to be used in homopolymerization was calculated according to the equations given below.

$$\text{mol of monomer} = \frac{\text{mass of monomer (g)}}{\text{Mw of monomer (g/mol)}} \qquad (6.1)$$

$$DP = \frac{\text{Mw of the polymer to be synthesized}}{\text{Mw of the monomer}} = n \quad (6.2)$$

$$DP = n = \frac{[\text{Monomer(g/mol) }]}{[\text{Catalyst(g/mol) }]} \quad (6.3)$$

$$\text{mass of catalyst(g)} = \text{mol of catalyst} \times \text{Mw of catalyst(g/mol)} \quad (6.4)$$

Where, DP means degree of polymerization. In our study these calculations were used for the synthesized polymers.

6.5 Synthesis of Polymers

6.5.1 Synthesis of *Exo*-Norbornene Polymer (Poly1-5k and Poly1-10k)

Polymerization has been done for two different molecular weights: 5,000 g/mol and 10,000g/mol, respectively. To produce 10,000 g/mol *Exo*-norbornene polymer (Poly1-10k) 200 mg of previously synthesized Monomer 1 was dissolved in 2 ml of DMF. 0.0088 g Grubbs 3rd generation catalyst dissolved in 200 μl of dichloromethane (DCM) was quickly added to the reaction medium in one shot and stirred under nitrogen for 2 hours. By adding 200 μl 30% ethyl vinyl ether (EVE) in DCM, polymerization was stopped and mixed for 30 minutes. The product, which was precipitated and washed in centrifuge 3 times using diethyl ether, was dried in a vacuum oven.

The same route has been followed to produce 5,000g/mol polymer using 0.0176 g Grubbs 3rd generation catalyst. (Poly1-5k) It has been observed that the anhydrite ring is easily affected by the humidity in the air, and it has been realized that sensitivity is required against moisture and working under inert atmosphere is necessary.

6.5.2 Synthesis of Oxanorbornene Polymer (Poly2-5k and Poly2-10k)

Polymerization has been done for two different molecular weights:5,000 g/mol and one for 10,000 g/mol, respectively. To produce 10,000 g/mol oxanorbornene polymer (Poly2-10k) 200 mg of furan maleic anhydride (Monomer 2) was dissolved in 2 ml of DMF. 0.017g Grubbs 3rd generation catalyst dissolved in 200 μl of DCM was quickly added to the reaction medium in one go and stirred under

nitrogen for 2 hours. By adding 200 μl 30% EVE in DCM, polymerization was stopped and mixed for 30 minutes. The product, which was precipitated and washed in centrifuge 3 times using diethyl ether, was dried in a vacuum oven.

The same route has been followed to produce 5,000 g/mol polymer using 0.0353 g Grubbs 3rd generation catalyst (Poly2-5k). It has been observed that the anhydrite ring is easily affected by the humidity in the air, and it has been realized that sensitivity is required against moisture and working under inert atmosphere nitrogen is necessary.

6.6 Hydrolysis of Polymers

To use the synthesized polymer in the sol-gel reaction, the polymer in the core must be able to interact with the SiO_2 shell formed by TEOS. For this reason, the anhydride ring in the structure of the polymer must be hydrolysed to obtain carboxylic acid functional group. We first used water to open anhydride ring of polynorbornene derivatives, however oxanorbornene skeleton preserve the ring opening quantitatively even after 4 day at room temperature.. In spite of that norbornene polymers were dissolved in couple of hours under the same condition. Thus we decided to use ammonia solution instead of water for the ring opening of anhydride functional group to end up with carboxylate anion. The aim is to form a carboxylic acid-ammonia salt structure further form sphere in solution after that the polymer can bond with the silanol groups obtained from TEOS. To hydrolyse the polymer quantitatively, 0.020 g each of all the synthesized polymers were dissolved separately with 1.1 ml of NH_4OH and left overnight to dissolve completely. Obtained products named as are Poly1H-5K, Poly1H-10k, Poly2H-5k, Poly2H-10k, respectively.

6.7 Sol-Gel Synthesis with Produced Polymers

The polymer dissolved in ammonia was slowly added dropwise to the flask containing 44 ml of ethanol, stirring at high speed. After mixing for 10 minutes, a total of 1.1 ml of TEOS was added to the medium in 5 times with an interval of 1 hour. For the hydrolysis reaction of TEOS to be completed, it was left for overnight

to mix at vigorous stirring. Solution was refluxed at 90 °C for 1.5 hours in order to remove ammonia from the mixture. The stock solution TEOS:EtOH:HCl:H_2O (1:23:0.2:12 by molar ratio) (2.68:16.11:0.07:2.59 by millilitres) prepared in a different container was added to the solution medium after mixing for 4 hours. All processes were repeated separately for 4 different polymers synthesized. Colour change, pH and particle size of the solution medium were monitored throughout the process. Coating was done with 4 different sol-gels which will be explained in detail under a separate heading. Flow chart of the mentioned sol-gel preparation process is given in Figure 6.1 below. Obtained sol-gels named as Sol1-5k, Sol1-10k, Sol2-5k, Sol2-10k respectively.

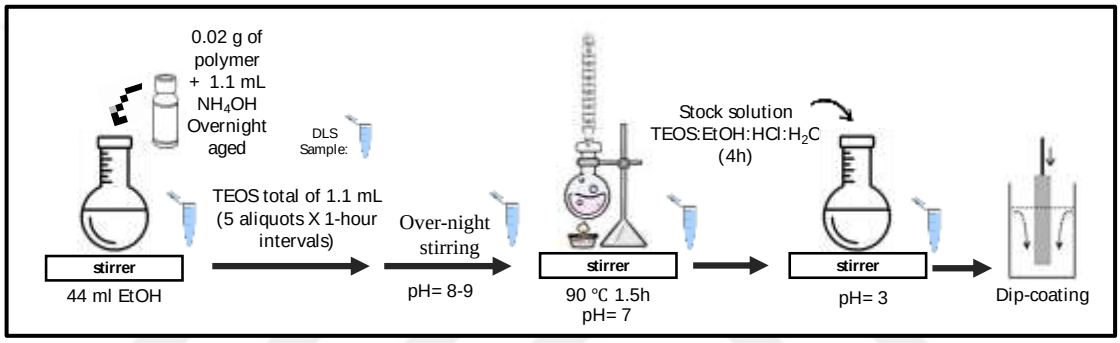

Figure 6.1 Sol-gel preparation process

6.8 Coating with Produced Sol-Gels

With the prepared different sol-gel, using the "KSV NIMA Dip Coater" device (4 x 10 cm^2) freshly cleaned "Sandy" glasses were coated. "Finnsonic" washing and drying tanks were used to wash the windows. The glasses are first left in the detergent added KOH solution in the cabinet ultrasonicated for 9 minutes. Then the glasses are immersed in the tank full of tap water. It is washed again with tap water after 9 minutes in an acid bath containing H_3PO_4. Then the glass is cleaned for the last time in two separate deionized water tanks one after the other. Each process takes 9 minutes and the temperature in all tanks is 60°C. After these processes, the glasses are dried at 100°C for 10 minutes. To cover only one surface of the glasses, one of the surfaces was processed after being covered with non-marking tape. The glasses were attached to the clamp of the device from the short side and immersed on the solution surface at an angle of 90° and constant velocity.

The device is positioned in a closed cabinet and the coating is done by following the ambient conditions to prevent air fluctuation by wind, temperature, and humidity changes during coating. After the coating process of the glasses was completed, they were kept in the ambient conditions in the cabin for 10 minutes, then they were cured in an oven at 100 °C for 10 minutes and finally tempered in a high-temperature oven at 700 °C for 3 minutes.

7
RESULTS AND DISCUSSION

7.1 Synthesis and Characterization of Monomers

7.1.1 Synthesis of (1R,2S,6R,7R)-4-oxatricyclo [5.2.1.$0^{2,6}$] dec-8-ene-3,5-dione

To obtain *exo* adduct of norbornene monomer ((2R,6S)-4-oxatricyclo [5.2.1.02,6] dec-8-ene-3,5-dione), first *endo*-norbornene is synthesized because *endo* products tend to be favoured in the Diels-Alder reaction mechanism and kinetically controlled [51]. Figure 7.1 shows the reaction mechanism of the *endo* intermediate product below. *exo*- norbornene can be thermodynamically produced from the *endo* product.

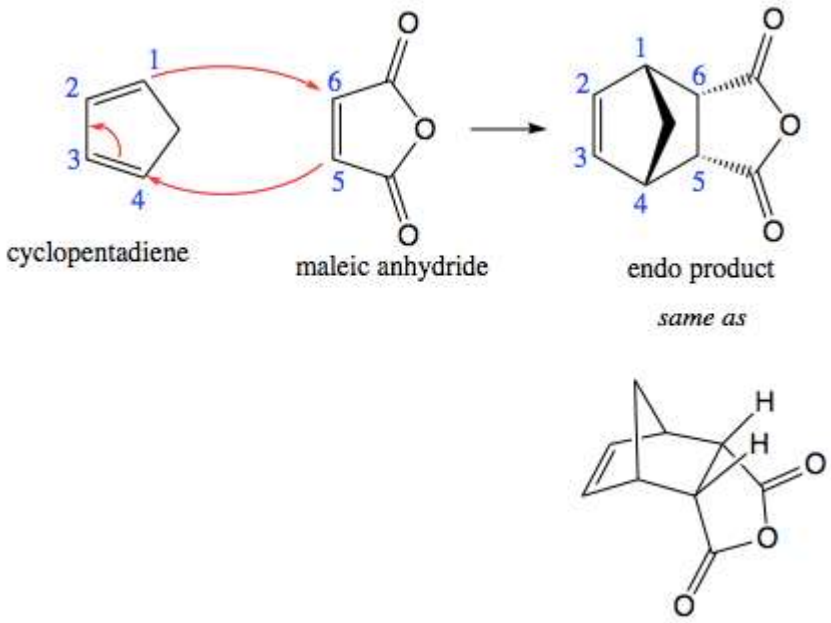

Figure 7.1 The Reaction mechanism of *endo* norbornene intermediate product

7.1.2 Synthesis of (2R,6S)-4-oxatricyclo [5.2.1.$0^{2,6}$] dec-8-ene-3,5-dione (Monomer 1)

To synthesize the *exo*-adducted norbornene monomer (M_W:164,16 g/mol) from *endo*, the *endo* product was kept under nitrogen atmosphere at 200 °C for 2 hours.

(Figure 7.2) Then the temperature was lowered to 120°C and toluene was added carefully. After that recrystallization process was applied a couple of times until no *endo* product residue remains in TLC purification controls (5 Hexane:1 Ethyl acetate) eventually white crystals obtained as *exo* adducted monomer. (M_W:166,13 g/mol)

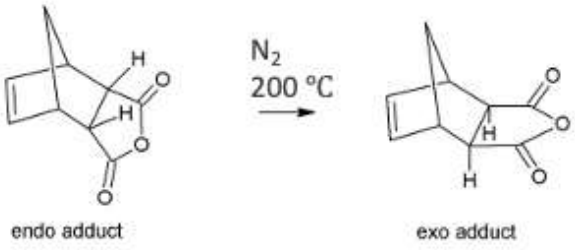

Figure 7.2 Reaction mechanism of Monomer 1

Synthesized Monomer 1 was characterized via FTIR and NMR. At the FTIR spectrum, (Figure 7.3) the characteristic strong peak at 1770 cm^{-1} represents the asymmetric C=O and the weak peak at 1828 cm^{-1} represents the symmetric C=O stretching of the carbonyl groups. There are some low-intensity peaks in the acidic -OH characteristic region at 2900 cm^{-1} [52]. This means that even though the monomer was kept in a sealed vial, it was observed that it is very air-moisture sensitive, and the anhydride ring slowly starts to break and turns into an acid functional group. Residual anhydride carbonyl strechings can still be seen at 1780 cm-1.

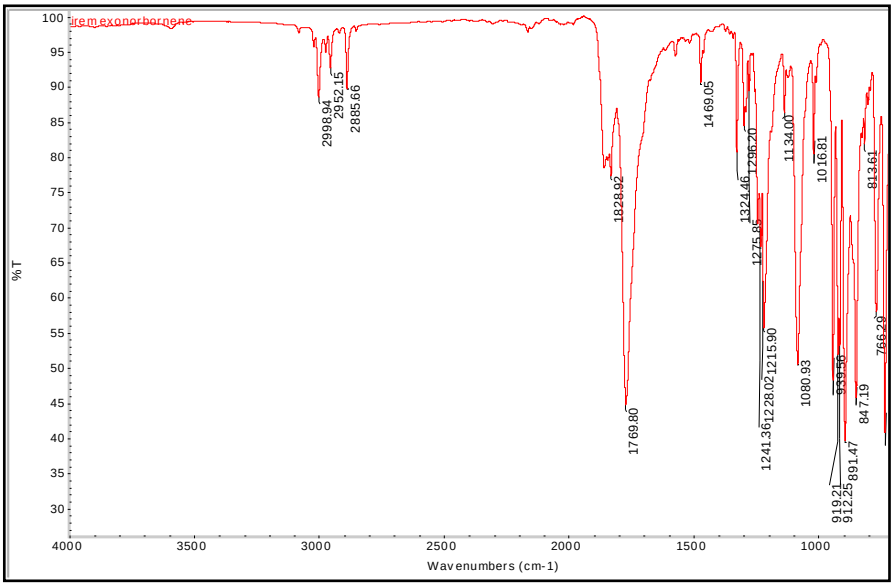

Figure 7.3 FTIR spectrum of Monomer 1

Monomer 1 was used as a model for the anhydride ring opening process. Thus, the monomer was dissolved in water analyzed in ^{13}C NMR. As seen in Figure 7.5, the characteristic carbonyl peak shifted from 173 ppm to 175 ppm when Monomer 1 was dissolved in water and the anhydride ring was opened.

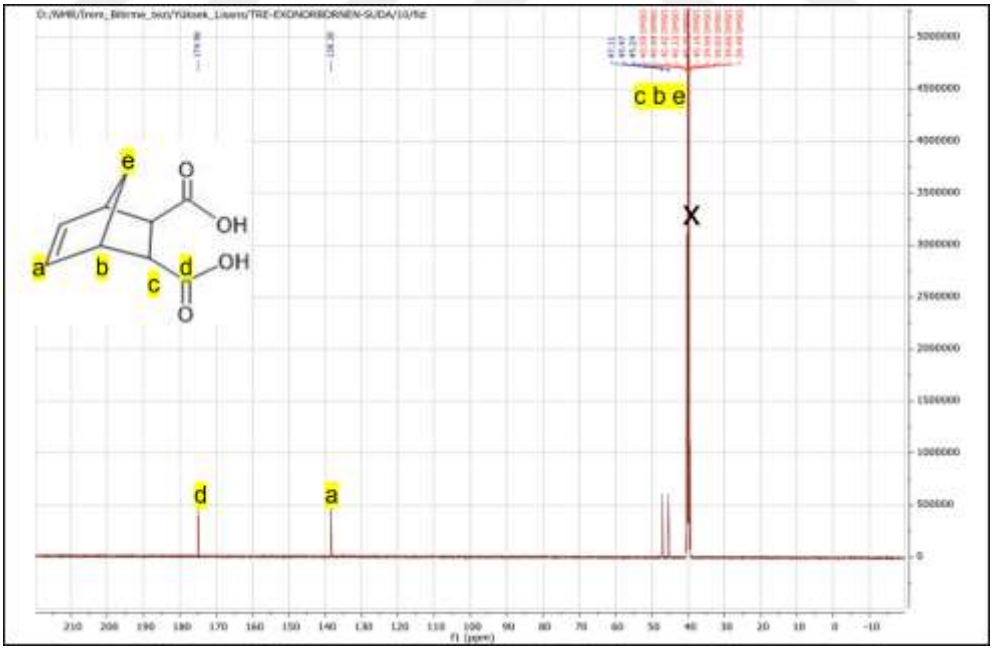

Figure 7.4 ^{13}C NMR spectrum of hydrolysed Monomer 1

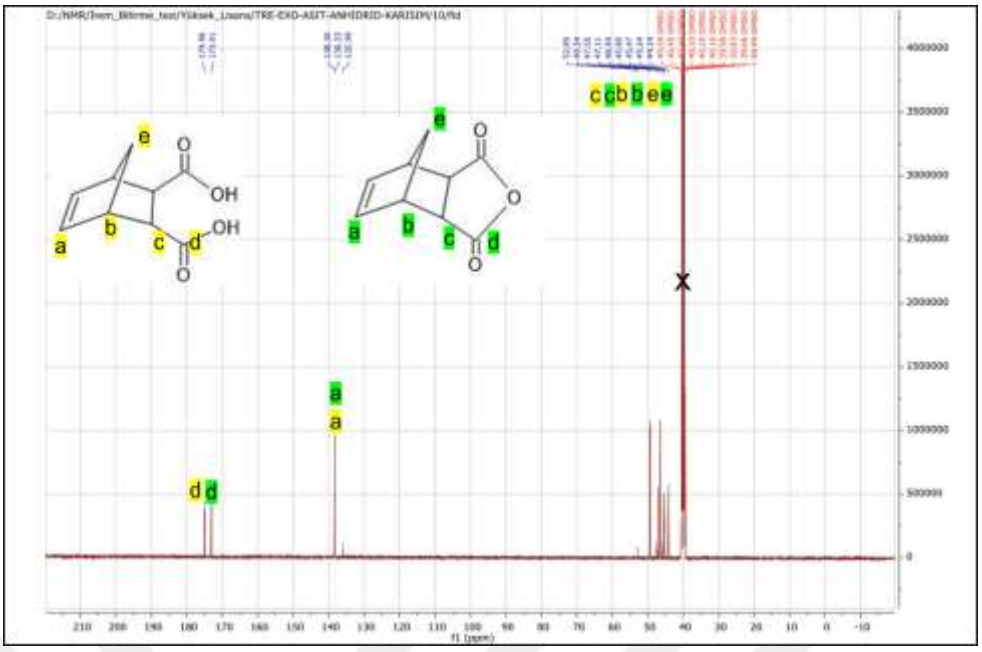

Figure 7.5 ^{13}C NMR spectrum of mixture of Monomer 1 and hydrolysed Monomer 1

However, solubility of Monomer 2 in water is not good and anhydride ring opening was not quantitative, we performed the ring opening with ammonia for all series of polymers.

7.1.3 Synthesis of Furan Maleic Anhydride Diels Alder Product (4,10-Dioxa-tricyclo [5.2.1.0] dec-8-ene-3,5-dione) (Monomer 2)

To synthesize Monomer 2, maleic anhydride and furan was conducted Diels-Alder reaction at room temperature. After 4 day pure white crystals (exo adduct) was observed in THF.

The synthesis of oxanorbornene (M_W:166,13 g/mol) via the Diels-Alder reaction between maleic anhydride and furan is shown in Figure 7.6. The ^{1}H NMR and the ^{13}C NMR spectra of Monomer 2 is shown in Figure 7.7 and Figure 7.8, respectively. Monomer 2 is shown to be in *exo* structure; the characteristic peaks of the *exo* stereoisomer structure was observed at 6.51 ppm on ^{1}H NMR spectrum for olefinic hydrogen and at 137 ppm on ^{13}C NMR spectrum for olefinic carbon. Characteristic carbonyl bond peak observed at 170 ppm on ^{13}C NMR spectrum [53].



Figure 7.6 The reaction route of the oxanorbornene monomer

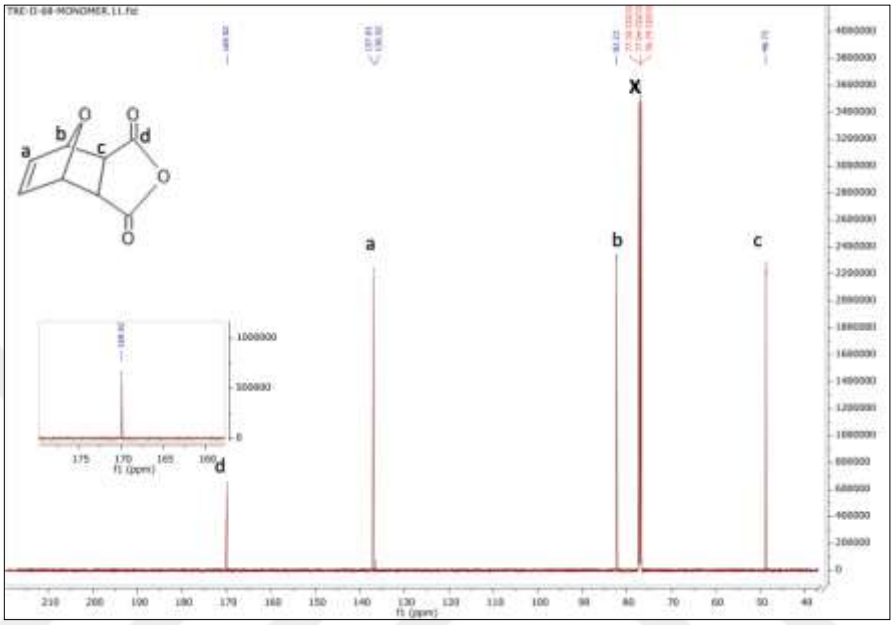

Figure 7.7 ^{13}C NMR spectrum of Monomer 2

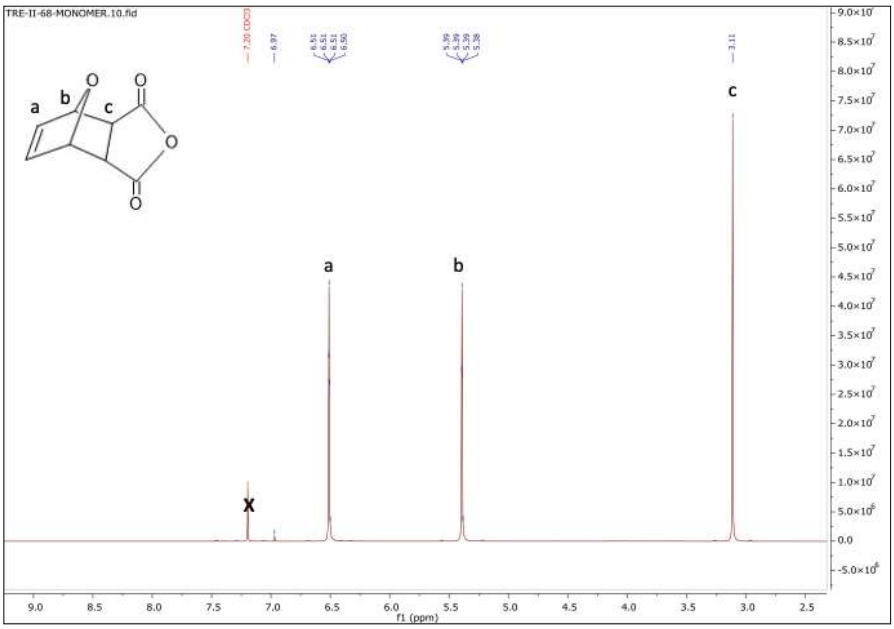

Figure 7.8 ^{1}H NMR spectrum of Monomer 2

Monomer 2 was also confirmed with FTIR analysis. For the cyclic anhydride structures, the characteristic strong peak at 1780 cm^{-1} represents the asymmetric C=O and the weak peak at 1855 cm^{-1} represents the symmetric C=O stretching of the carbonyl groups. To determine whether the structure is cyclic anhydride the low wavenumber of these carbonyl groups must have stronger intensity. In Figure 7.9 it can be seen the 1780 cm^{-1} stretching is much stronger than in 1855 cm^{-1}. The strong stretching of the C-O bond can be seen between 1300-1100 cm^{-1} for cyclic anhydride structures. Here, stretching was observed at 1214 cm^{-1}.

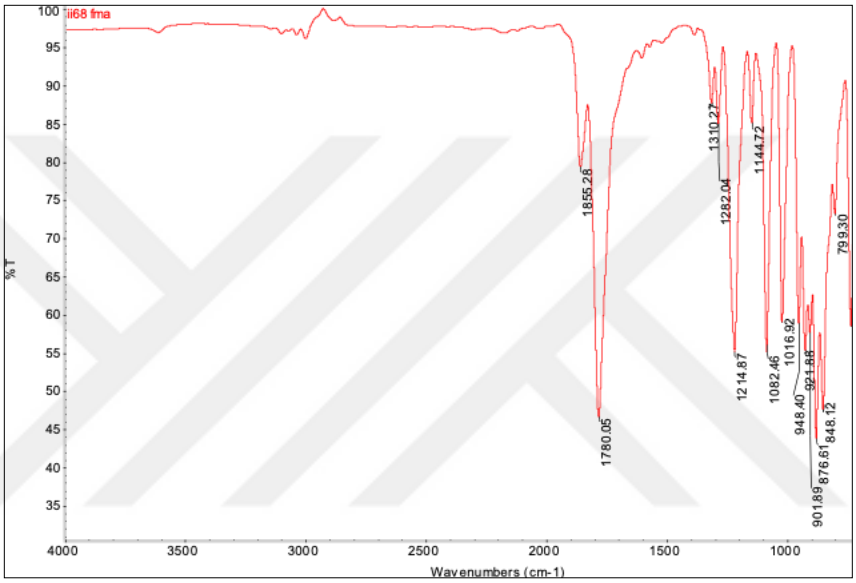

Figure 7.9 FTIR spectrum of Monomer 2

7.2 Synthesis and Characterization of Polymers

7.2.1Synthesis of *Exo*-Adducted Norbornene Polymer (Poly1-5k and Poly1-10k)

Polymerization was applied according to the literature [54],[55]–[57]. Polymerization has been done for two different molecular weights; 5,000g/mol (Poly1-5k) and one for 10,000g/mol (Poly1-10k), respectively. (Figure 7.10) The same reaction routes is used for the synthesis of both polymers except catalyst quantity in each experiment. To produce *Exo* adducted norbornene polymer, Monomer 1 was dissolved in DMF and Grubbs 3rd generation catalyst was added after dissolving in small amount of DCM. Polymerization was stopped by ethyl vinyl ether after 2 h. After work up, oven brown solid polymers were obtained

quantitively. Polymers were kept under inert atmosphere and dessicator due to the sensitivity of the anhydride ring against to moisture.

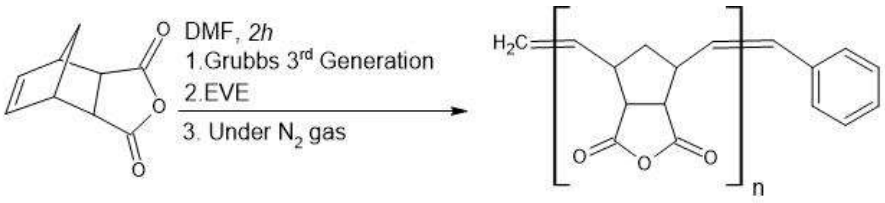

Figure 7.10 Synthesis route of *exo*-norbornene polymer

The ^{1}H NMR and the ^{13}C NMR spectra of Poly1-5k are given below respectively. In Figure 7.11. The carbonyl group's characteristic peak observed at 173 ppm on ^{13}C NMR spectrum. In the ^{13}C NMR analysis, the broken double bond carbon peaks in the oxanorbornene ring were observed at 132 ppm. The residual solvent was also observed in the spectrum.

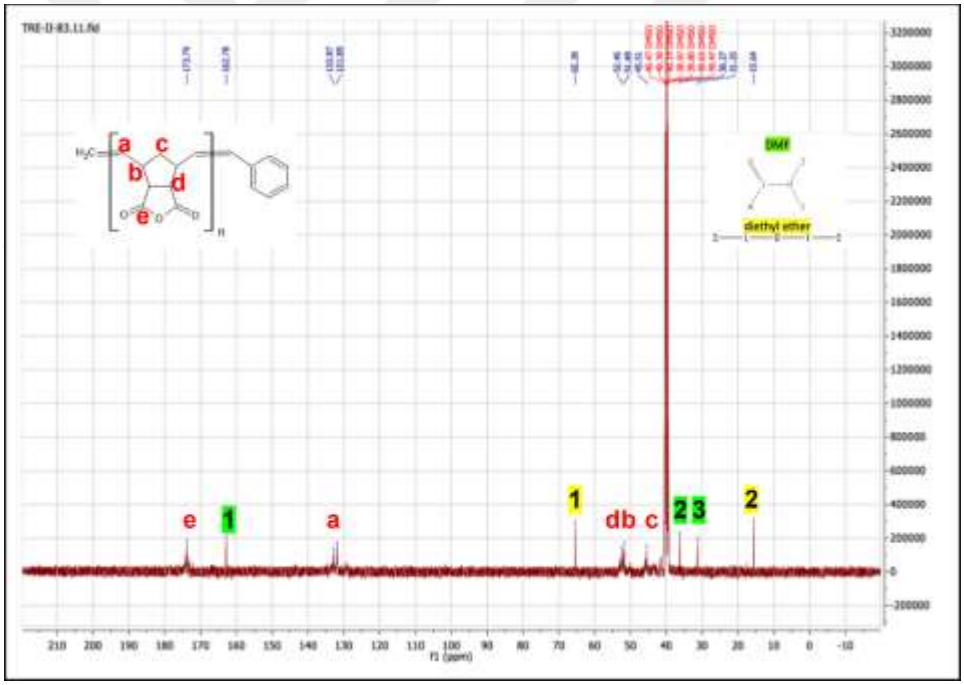

Figure 7.11 ^{13}C NMR spectrum of Poly1-5k

The cis/trans protons (a) of polymer are seen at approximately 5.5 ppm as broad at ^{1}H NMR spectrum (Figure 7.12). , ^{1}H and ^{13}C NMR spectra of Poly1-10k were given in Figure 7.13 and Figure 7.14, respectively. However, characterization will not be explained in detail due to the structural similarity with Poly1-5k.

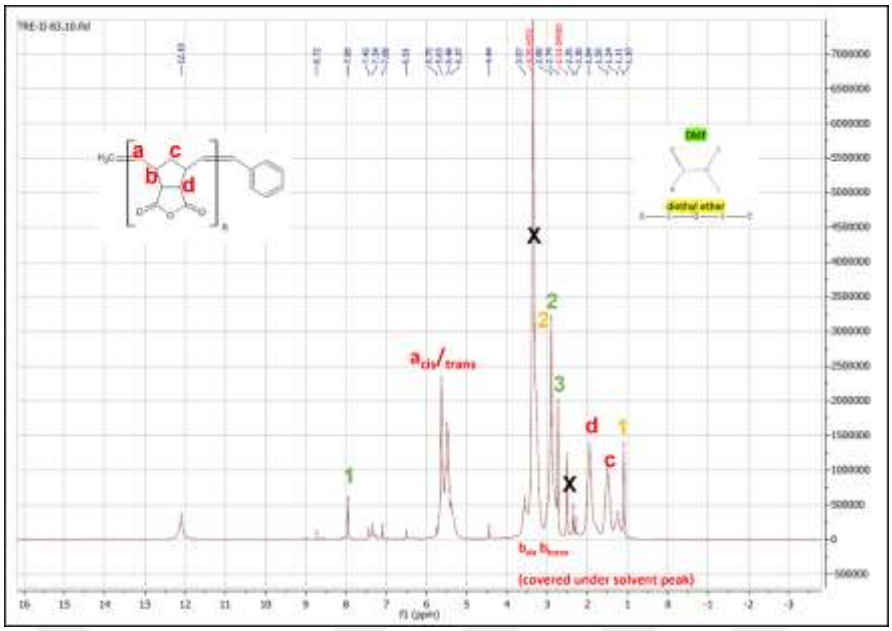

Figure 7.12 ^{13}H NMR spectrum of Poly1-5k

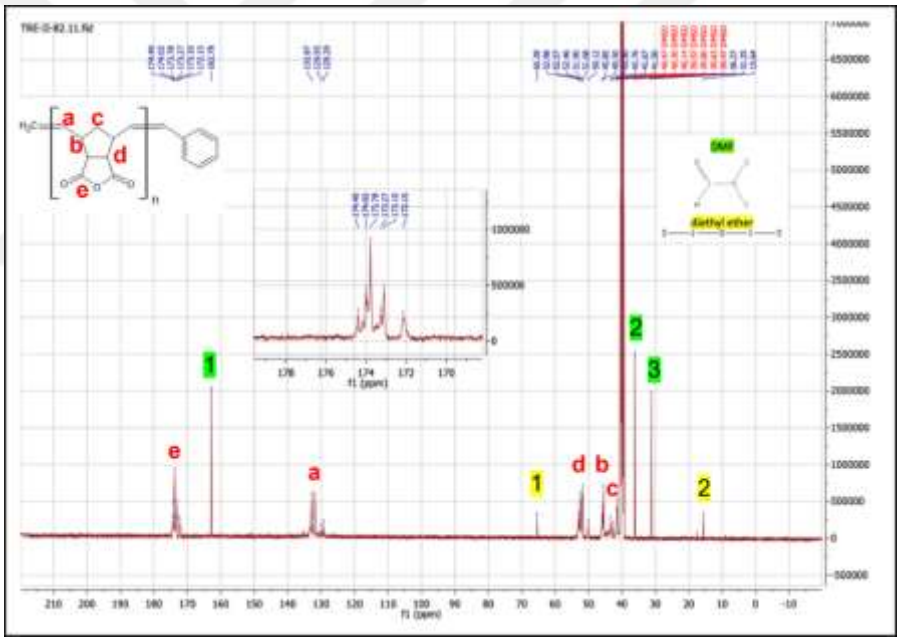

Figure 7.13 ^{13}C NMR spectrum of Poly1-10k

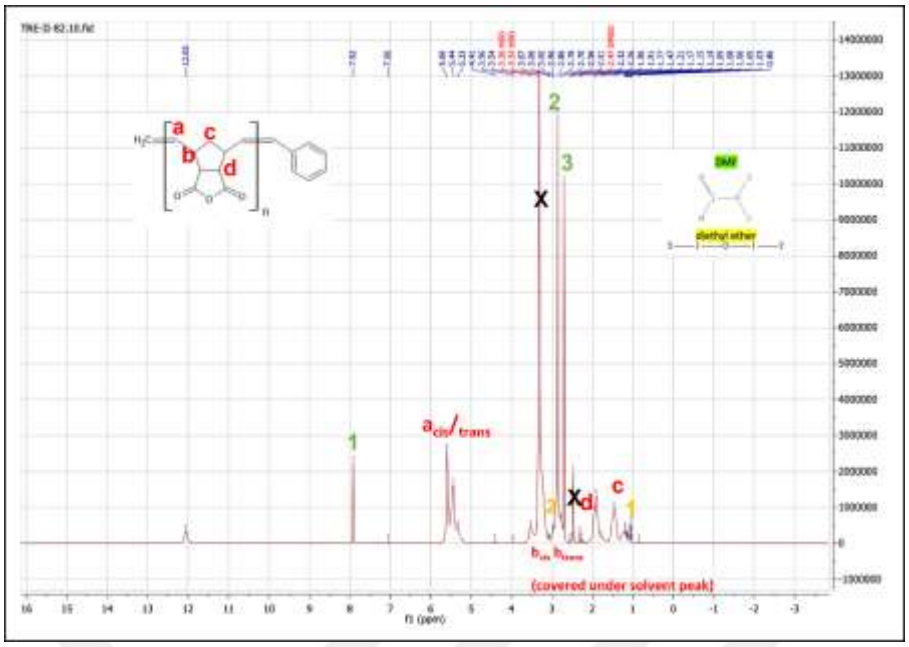

Figure 7.14 ^{13}H NMR spectrum of Poly1-10k

Both for the Poly1-5k and Poly1-10 k, the cyclic anhydride structures, the characteristic strong peak at 1772 cm^{-1} represents the asymmetric C=O and the weak peak at 1857 cm^{-1} represents the symmetric C=O stretching of the carbonyl groups in Figure 7.15 and Figure 7.16. The stretching of the C-O bond can be seen between 1300-1100 cm^{-1} for cyclic anhydride structures. Here, we observed this stretching at 1210 cm^{-1}

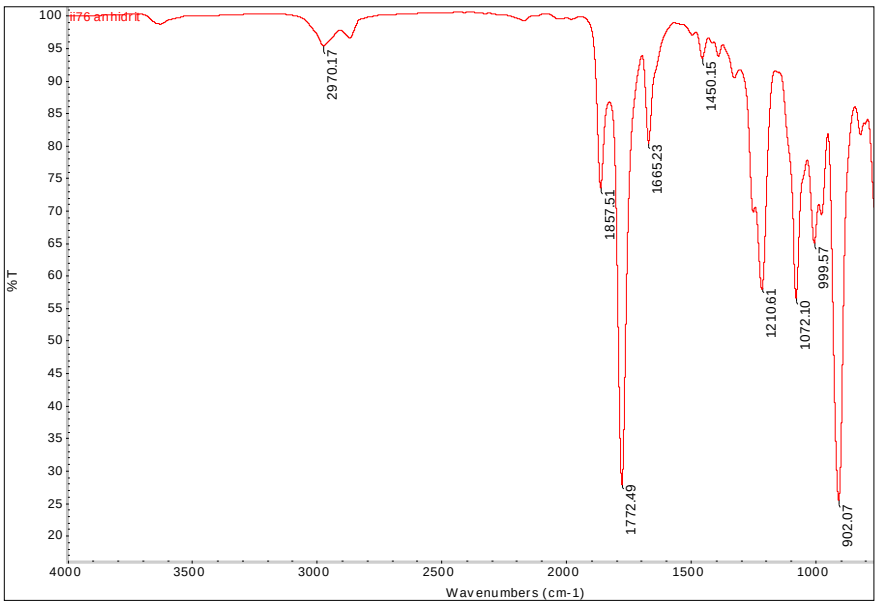

Figure 7.15 FTIR spectrum of Poly1-5k

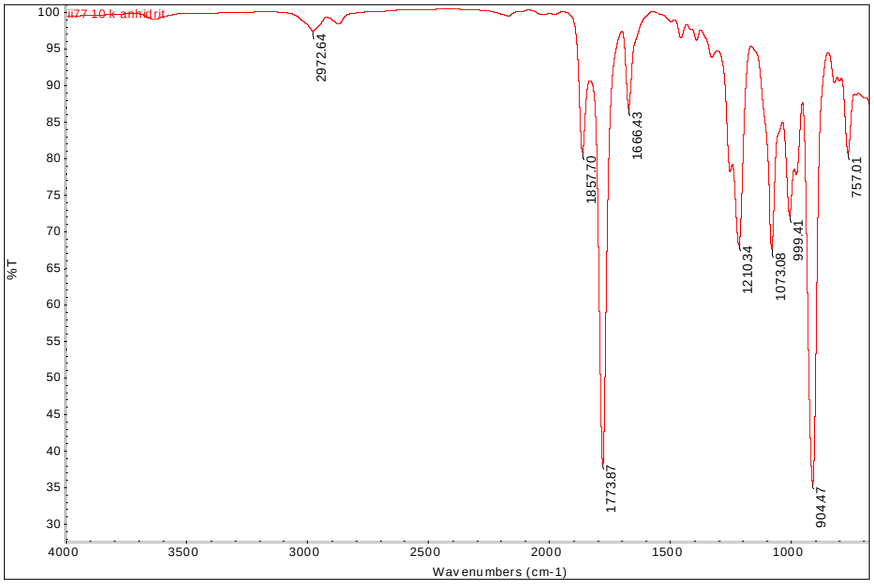

Figure 7.16 FTIR spectrum of Poly1-10 k

7.2.1.1 Hydrolysis of Norbornene Polymers (Poly1H-5k and Poly1H-10k)

The anhydride ring in the structure of the polymer is opened with the help of ammonia and thus the polymer is hydrolyzed. To achieve that the synthesized polymers were dissolved separately with NH_4OH and left overnight to dissolve fully. Obtained products named as Poly1H-5k, Poly1H-10k respectively. Figure 7.17 shows the reaction mechanism.

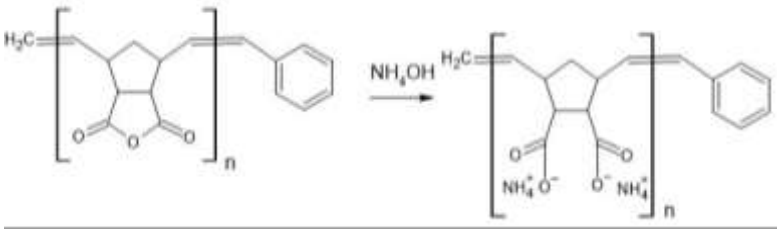

Figure 7.17 The hydrolysis reaction mechanism of Poly1-5k & Poly1-10 k

The ^{13}C NMR spectra of Poly1H-5k is shown in Figure 7.18. The formation of carboxylic acid-ammonia salt was observed at 174 ppm for C(=O) as multiplet. The residual solvent (DMF and diethyl ether) were also observed in the spectrum due to the poor vacuuming process after workup.

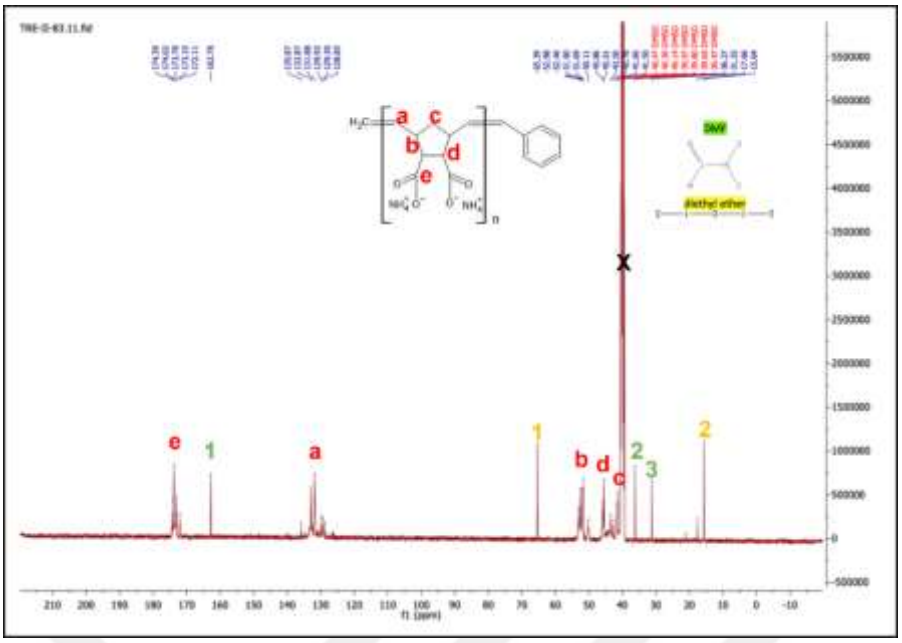

Figure 7.18 ^{13}C NMR spectrum of Poly1H-5k

When polymers dissolved in ammonia, anhydride ring is opened and the characteristic strong peak at 1780 cm^{-1} that represents the asymmetric C=O and the weak peak at 1855 cm^{-1} the symmetric C=O stretching of the carbonyl groups disappear and a stretching appears at 1650 cm^{-1} due to the NH_4^+bonding of the new acid functional group carbon. It can be seen in the Figure 7.19 the red graph lines represents the Poly1-5k and the turquoise lines Poly1H-5k. Same shift was also observed in Poly1-10k when it turns into Poly1H-10k in Figure 7.20. Also, the characteristic acidic stretch between 3000-3200 cm^{-1} can be seen in both spectra.

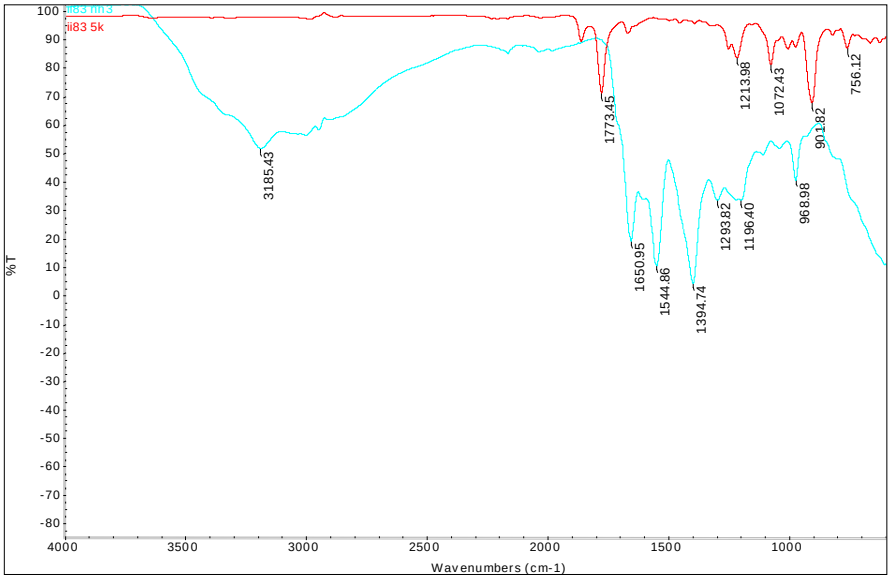

Figure 7.19 FTIR spectrum of Poly1-5k (red) and Poly1H-5k (turquoise)

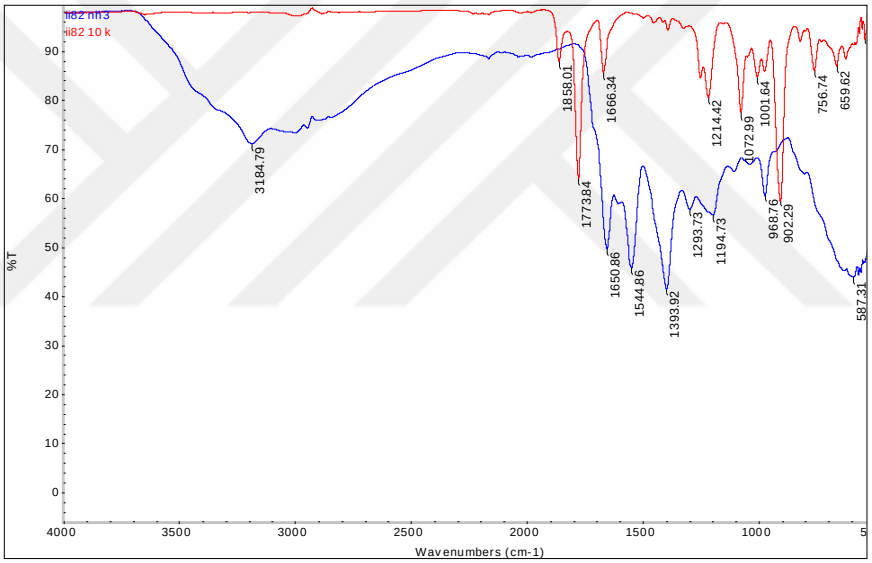

Figure 7.20 FTIR spectrum of Poly1-10k (red) and Poly1H-5k (blue)

7.2.2 Synthesis of Oxanorbornene Polymer (Poly2-5k and Poly2-10k)

Polymerization has been done for two different molecular weights; one for 5,000g/mol and one for 10,000g/mol. In a typical example, To produce 10,000 g/mol oxanorbornene polymer (Poly2-10k), furan maleic anhydride adduct (monomer 2) was dissolved in DMF and Grubbs 3rd generation catalyst was inserted in one shot after dissolving in minimum amount of DCM. Polymerization was stopped by adding ethyl vinyl ether. (Figure 7.21). The same route has been followed to produce 5,000 g/mol polymer using Grubbs 3rd generation catalyst

(Poly2-5k). Polymers were kept under inert atmosphere and dessicator due to the sensitivity of the anhydride ring against to moisture. .[58]

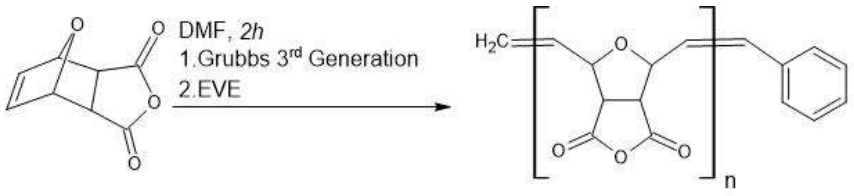

Figure 7.21 Synthesis route of oxanorbornene polymer

The ^{13}C NMR and the ^{1}H NMR spectra of Poly2-5k is shown in Figure 7.22 and Figure 7.23, respectively. The characteristic peak for anhydride carbonyl was observed at 170 ppm at ^{13}C NMR spectrum. The peak at 172 nm shows the shifting back of the signal due to the anhydride ring opening. This is because the anhydride ring opened due to the moisture sensitivity. In the ^{13}C NMR analysis, cis and trans double bond carbon peaks (C=C) were observed at 129-130 ppm. The residual solvent also observed in the spectrum due to the poor vacuuming process before after workup.

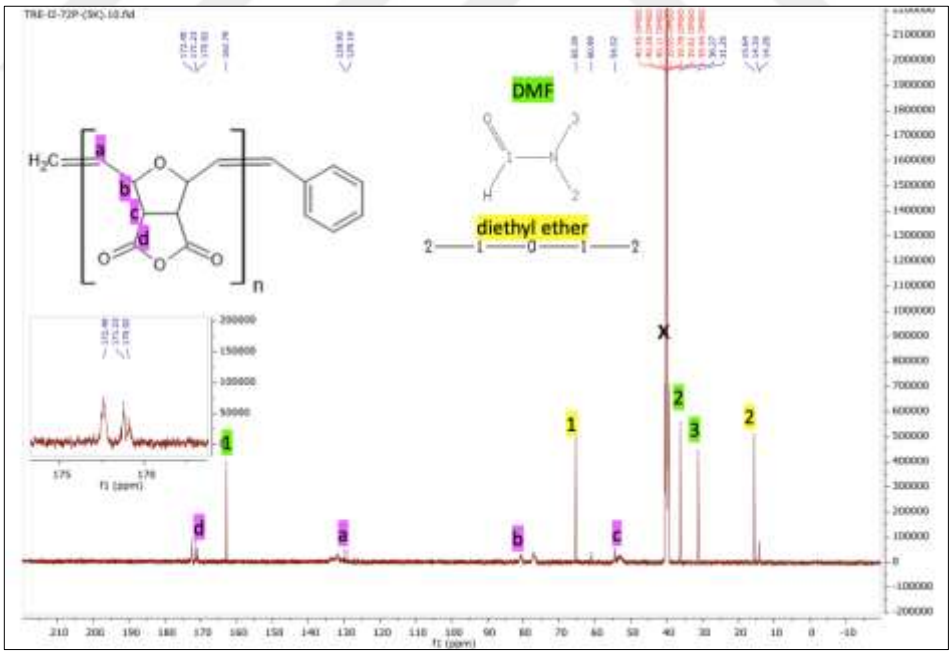

Figure 7.22 ^{13}C NMR spectrum of Poly2-5k

the cis/trans protons (a) of the polymers were observed at 6.0 ppm as broad. Ring protons (CH-O) were around 5.0 ppm (b_{cis}), and 4.5 ppm (b_{trans}) on ^{1}H NMR spectrum. (Figure 7.23)

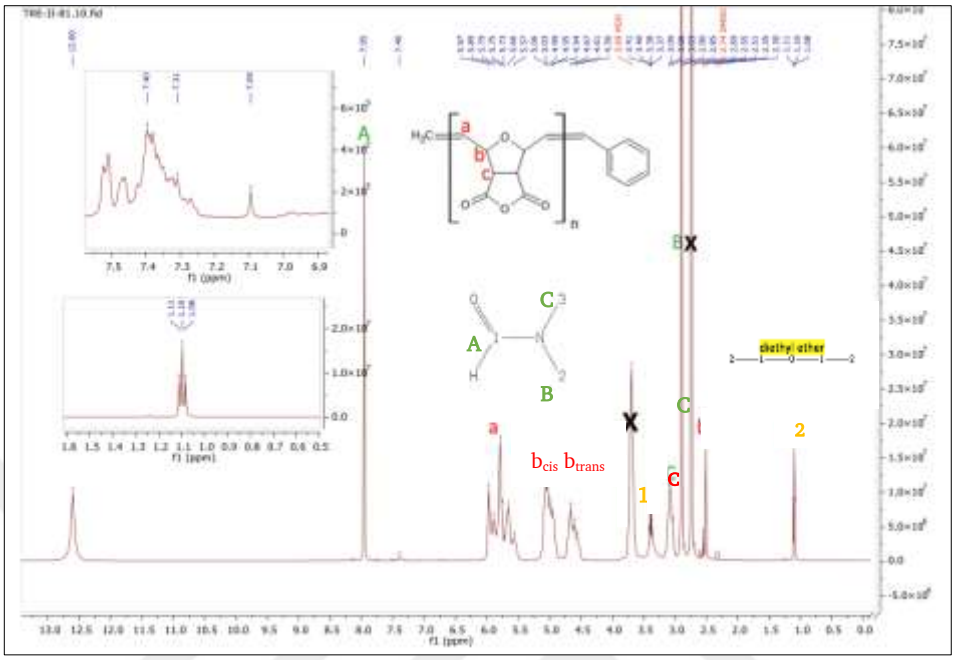

Figure 7.23 ^{1}H NMR spectrum of Poly2-5k

FTIR analysis is also confirmed the polymers (Figure 7.24 and Figure 7.25). The cyclic anhydride structures, the characteristic strong peak at 1776 cm^{-1} represents the asymmetric C=O and the weak peak at 1865 cm^{-1} represents the symmetric C=O stretching of the carbonyl groups in. The stretching of the C-O bond can be seen between 1300-1100 cm^{-1} for cyclic anhydride structures. This stretching was observed at 1220 cm^{-1} for Poly2-5k and Poly2-10k

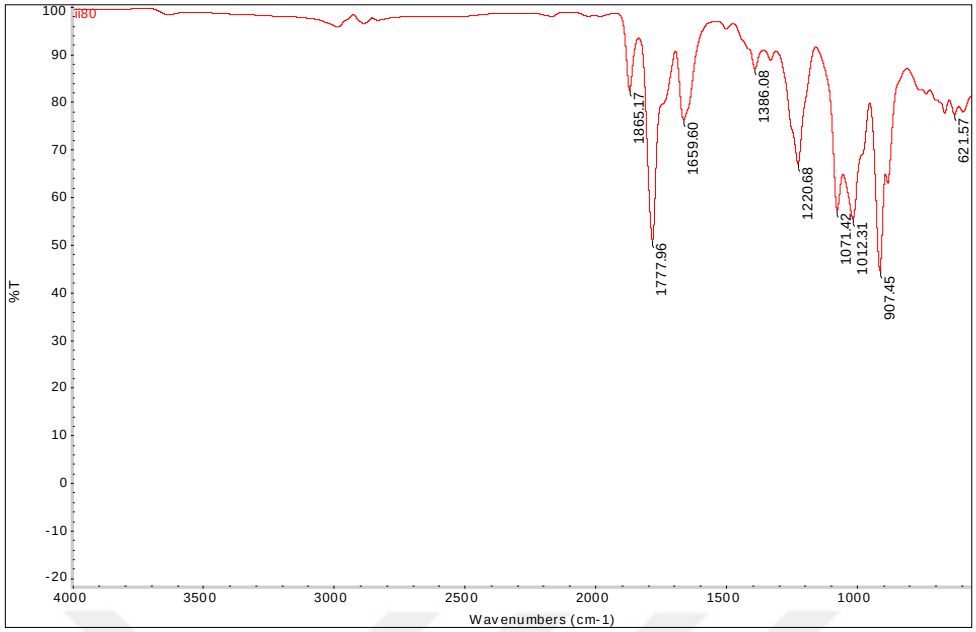

Figure 7.24 FTIR spectrum of Poly2-5k

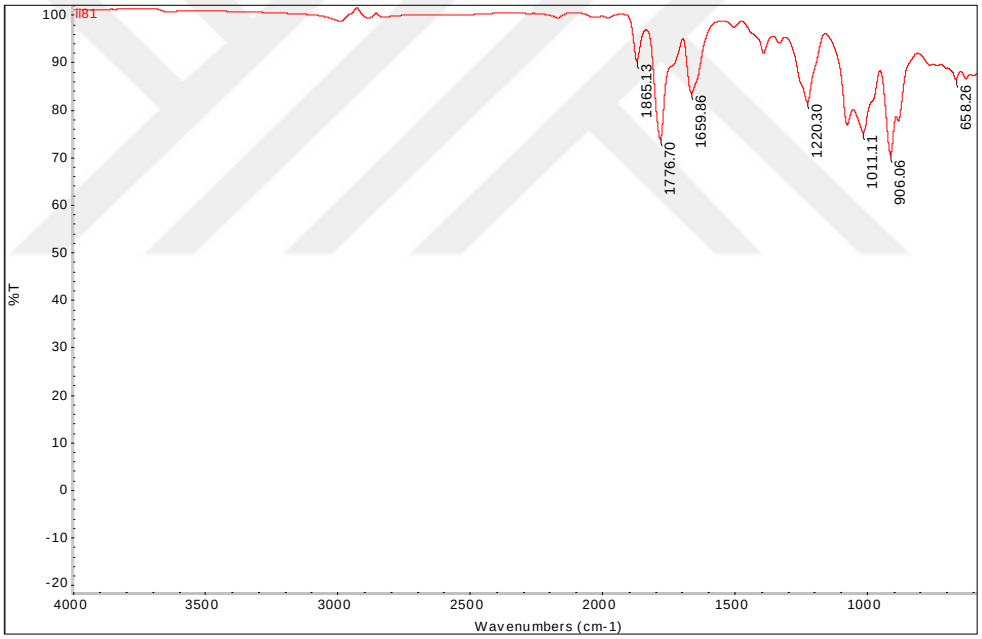

Figure 7.25 FTIR spectrum of Poly2-10k

7.2.2.1 Hydrolysis of Oxanorbornene Polymers (Poly2H-5k and Poly2H-10k)

The anhydride ring in the structure of the polymer is opened with the help of ammonia and thus the polymer is hydrolyzed to form carboxylate-ammonia salt. To achieve that the synthesized polymers were dissolved separately with NH_4OH

and left overnight to dissolve completely. Obtained products are named as Poly2H-5k, Poly2H-10k respectively. Figure 7.26 shows the reaction mechanism.

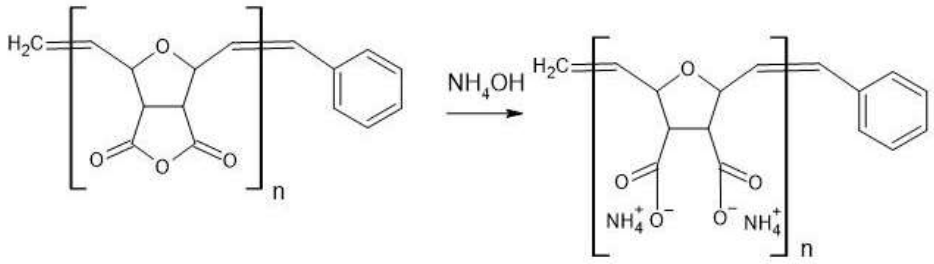

Figure 7.26 The hydrolysis reaction mechanism of Poly2-5k & Poly2-10 k

When the polymer was dissolved in ammonia, it was expected to open the anhydride ring and form a polyelectrolyte structure with NH_4^+. Accordingly, characteristic carbonyl peak of anhydride ring of polymer was observed at 172 ppm as it is explained before. A shift to 175 ppm is observed in ^{13}C NMR spectrum (Figure 7.27) when the ring opens with ammonia.. The residual solvent was also observed in the spectrum due to the poor vacuuming process after workup.

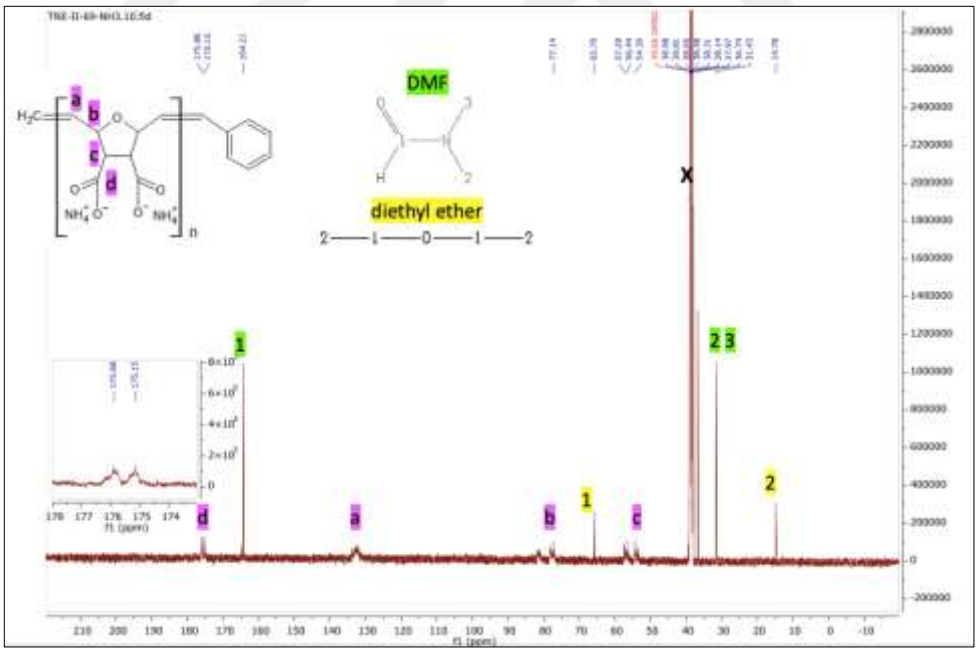

Figure 7.27 ^{13}C NMR spectrum of Poly2H-5k

FTIR analysis is also confirmed the products. When polymers were dissolved in ammonia, anhydride ring is opened and the characteristic strong peak at 1780 cm

[1] that represents the asymmetric C=O and the weak peak at 1855 cm^{-1} the symmetric C=O stretching of the carbonyl groups disappeared and a stretching appeared at 1650 cm^{-1} due to the NH_4^+bonding of the new acid functional group carbon. It can be seen in the Figure 7.28 the blue graph lines represents the Poly2-5k and the red lines Poly2H-5k. Same shift was also observed in Poly2-10k when it turns into Poly2H-10k in Figure 7.29. Also, the characteristic acidic stretch between 3000-3200 cm^{-1} can be seen in both spectra.

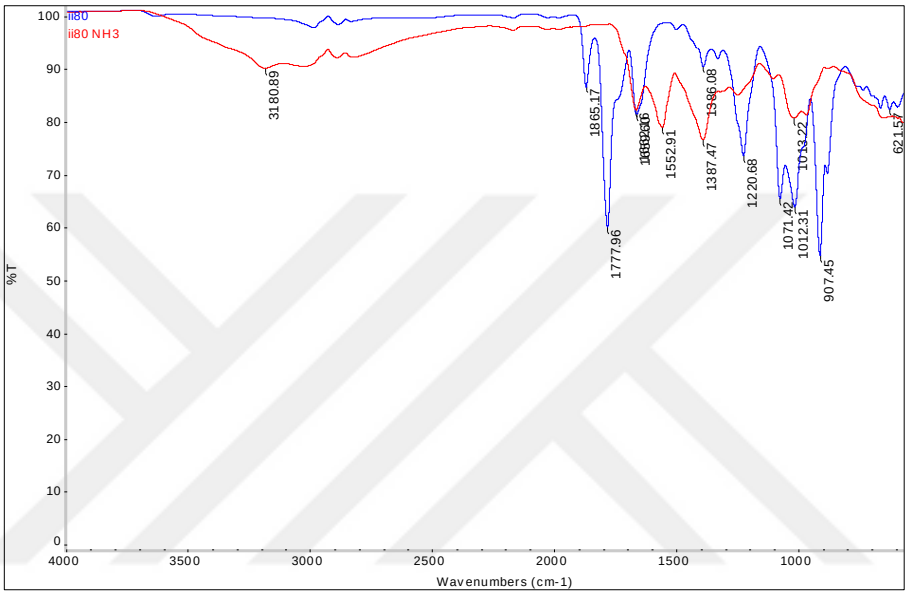

Figure 7.28 FTIR spectrum of Poly2-5k (blue) and Poly2H-5k (red)

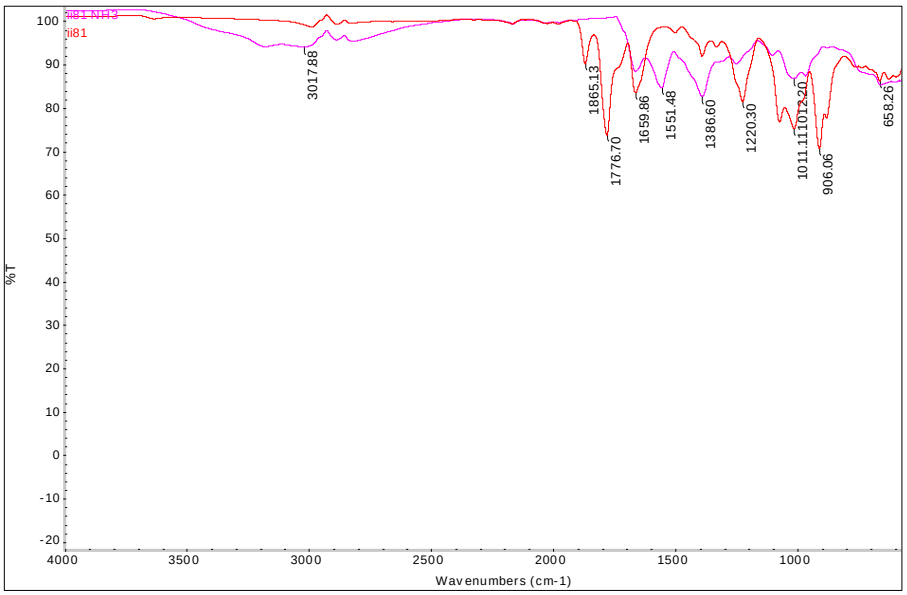

Figure 7.29 FTIR spectrum of Poly2-10k (blue) and Poly2H-10k (red)

7.2.3 Molecular Weight Distribution of Polymers

The polymer molecular weight distribution analyses were determined by gel permeation chromatography (GPC) and end group analysis via ^{1}H NMR in Table 1. M_n analyzes that made from the ^{1}H NMR spectrum of the polymers via end group analysis. Phenyl rings which is present at the end group of polymer chain possess 5 protons, was observed at around 7.95 ppm. The a_{cis} proton comes in between 5.5-6.0 ppm and has 2 protons. Integrate these two protons over the spectrum, and multiplying the ratio of the integrals per proton to each other by the molecular weight of the monomer gives us the molecular weight (M_n) of the polymer. For example, the phenyl ring integral of the Poly1-5k polymer is taken 1 as a reference (Figure 7.14). Phenyl ring has 5 protons in its structure. Therefore, the integral result is divided by 5 and the integral value per proton is found to be 0.2.The integration of $a_{cis/trans}$ protons is determined as 19.51, but it is the value of 2 protons in total. So the value of a proton is 19.51/2 equals to 9.755. When this value is proportional to the value per proton of the reference phenyl ring, the result is 48,775. This equals to the repeating unit of the integrated polymer and when we multiply the integration ratio with molecular weight of the repeating unit, Mn of the polymer can be obtained.

Table 7.1 Molecular weight distribution

	$M_{n\ Theoritical}$	$M_{n,\ NMR}$	$M_{n,\ GPC}$	$M_{w,\ GPC}$	$PDI_{\ GPC}$
Poly1-5k	5,000	8,006	24,545	25,575	1.042
Poly1-10k	10,000	22,120	44,239	47,735	1.079
Poly2-5k	5,000	7,347	31,739	130,621	4.115
Poly2-10k	10,000	12,659	176,105	189,323	1.075

$M_{n,Theoretical}$: Theoretical number average molecular weight (Da)

$M_{n,NMR}$: Average molecular weight calculated by ^{1}H NMR (Da)

$M_{n,GPC}$: Number average molecular weight with GPC (Da)

$M_{w,GPC}$: Weight average molecular weight with GPC (Da)

PDI: Polydispersity index obtained from GPC

GPC was performed using aq mobile phase (0.1 M AcOH, 0.15 M NaCl) and polyethylene glycol standart was used as a calibration standart.

Targeted and observed molecular weights deviate from each other. Here we conducted polymerization under DMF and DMF is not a proper solvent for metathesis polymerization using Grubbs catalyst. Residual amines can inhibit the catalyst efficiency in some amount. Thus, we observed some deviation as it can be seen in Table 1. For example targeted molecular weight for Poly1-10 k was 10,000 g/mol but M_n analysis showed the molecular weight is 22,120 g/mol. Deviation in Poly 2 series is more dramatic. GPC spectrum showed bimodal peak formation and high molecular weight (> 100 000 g/mol). This might be due to the improper solvent for the solubilize the polymer in mobile phase and formation of aggregate with possesing larger hydrodynamic volume. It should also be point out that PEG is used for the calibraton standard, more proper calibration standard to compare the acrylic acid salt bearing polymer can also be used for the proper analysis. Further analysis might be done using MALDITOFF and zeta sizer to speculate about the molecular weight of the polymers.

7.2.4 Thermal Properties of Synthesized Polymers

TGA analyses were done to determine the char yield of the polymers and thermal analysis was done under nitrogen atmosphere. Char yields from TGA values were calculated for *exo*-norbornene polymers, Poly1-5k, and Poly1-10k, Oxanorbornene polymers Poly2-5k, and Poly2-10k respectively. It was observed that Poly1-5k has the highest char yield (29.20%). (Figure 7.30) Other polymers' char yields are 28.03% (Poly1-10k), 27.19% (Poly2-5k), 25.56% (Poly2-10k) respectively.

It was observed in TGA graph that decomposition started at approximately 300 °C. . This is basically result from the chain end of the polymers. Lower molecular weighted polymers (Poly1-5k and Poly2-5k) have a greater number of chain end in the same amount of sample. Thus, first decomposition cycle is more pronounced effect. In addition, when the results were compared in terms of Poly1 and Poly2

series, Poly1 series left more char yield because of the structure of norbornene produce carbon char residues against oxygen bearing skeleton.

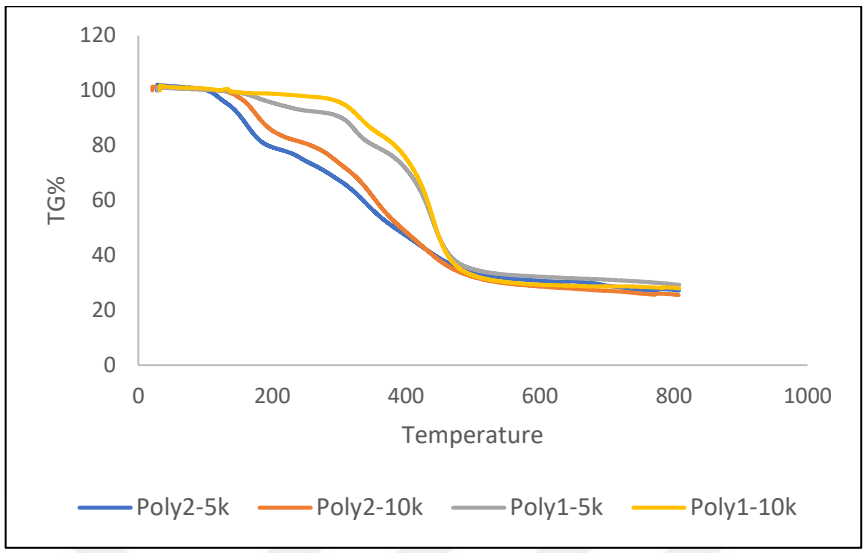

Figure 7.30 Nitrogen TGA graph of the synthesized polymers

7.3 Sol-Gel Synthesis and Characterization with Hydrolysed Polymers

7.3.1 Sol-gel Synthesis (Sol1-5k, Sol1-10k, Sol2-5k, Sol2-10k)

The polymer dissolved in ammonia was slowly added dropwise to ethanol, stirring at high speed. After mixing for 10 minutes, TEOS was added to the medium in 5 times with an interval of 1 hour. For the hydrolysis reaction of TEOS to be completed, it was left for overnight to mix at vigorous stirring. In order to remove ammonia in the environment, it was refluxed. The stock solution TEOS:EtOH:HCl:H_2O prepared in a different container was added to the solution medium after mixing for 4 hours. All processes were repeated separately for 4 different polymers synthesized. The core-shell formation illustrated in Figure 7.31 below.

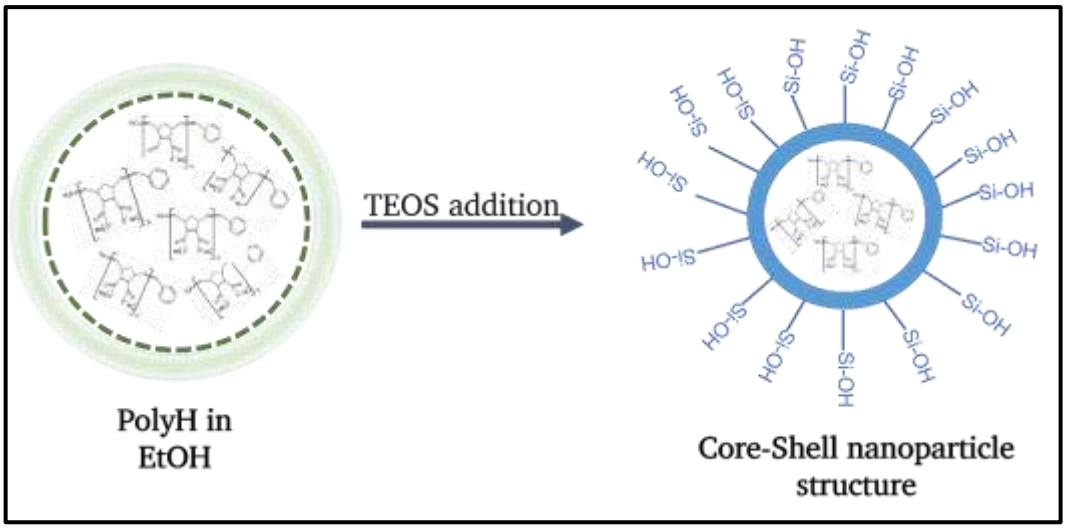

Figure 7.31 Core-shell formation via polynorbornene series

7.3.2 Nanoparticles Size Distribution via DLS

Dynamic light scattering (DLS), also known as Quasi-elastic light scattering, is a well-known, non-invasive technique for determining the size and size distribution of molecules and particles in the submicron range and below 1 nm. It is based on the Brownian motion of dispersed particles in a liquid which they move randomly in all directions. Characterization of particles, emulsions, or molecules that have been distributed or dissolved in this type of liquid is the typical use of dynamic light scattering. Laser light is scattered at different intensities due to the Brownian motion of particles or molecules in suspension. Backscattered light is detected and measured to obtain the Particle Size Distribution (PSD) by means of intensity, volume or number [59]–[61].

ZetaSizer is an instrument that can measure and analyze the particle size, zeta potential and molecular weight of the colloidal diluted materials. The main working principle is shown in Figure 7.32.

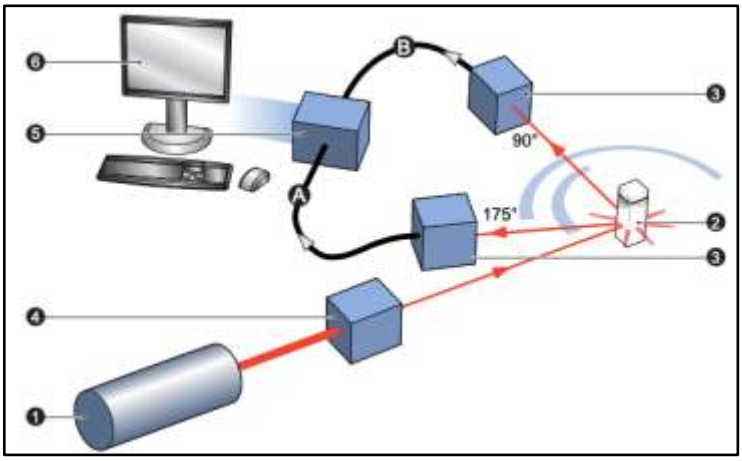

Figure 7.32 A typical DLS system 1) laser 2) cell 3) detector 4) attenuator 5) correlator 6) computer

In order to monitor the particle size at each step during the sol-gel preparation, 2 ml samples were taken for ZetaSizer. The sample was passed through a 0.45 micron filter and particle size analysis was performed in ZetaSizer with 173° backscatter angle in polystyrene disposable cuvettes.

The general trend expected in particle size measurements in our study is that it first increases and then remains constant. Since the polymer surface is modified with SiO_2 shell by adding TEOS after the first measurement, the particle size increases in the Pre-Reflux stage, and then continues in the same way until the end of the process with constant or small changes as much as possible. Another parameter as important as the particle size is the polydispersity index (PdI), which indicates that as PdI approaches 0 in the measurement taken, it has a monodisperse structure. This value approaches 1 if there is more than one particle size distribution in the sample. Thus, it can be seen how narrow particle size distribution or how many dominant populations are present in the sample. Generally, <0.400 means monodispersity.

Table 2 shows the particle size distribution. According to results, inconsistencies were observed in the particle sizes of the samples taken during the process in the sol-gels prepared with norbornene polymer (Sol1 5k and Sol1 10k). Probably due to the charge from NH_4^+ in the polymer structure, it first created a large template such as 507 and 423 nm in Sol1 series. It was observed that the particle size

decreased while NH_4^+ was displaced by newly formed SiO_2 bonds. This may be due to the fact that the hydrolysis reaction of TEOS is a fast reaction, and it splits the templates into smaller pieces while displacing with ammonia, creating more stable, spherical particles. Thus, after the SiO_2 shell formed around the polyelectrolyte due to gradually added TEOS, particle size decreases. But still, this is an inconsistent result when it compared to especially Sol2-5k result.

For both different chain lengths in Sol1 series, as it can be seen from the graph in Figure 7.33 and Table 2 it became to a same nanoparticle size with same distribution.

Sol2 5k and Sol2 10k on the other hand, according to the Figure 7.34-35-36 and Table 2 it was observed that more than one dominant particle size population was formed in the Sol2 10 k coded sol-gel with a longer chain length after TEOS added into the sol. The reason for this may be that the TEOS added when a template is desired to be made with a high molecular weight polymer is not sufficient and cannot completely wrap around the polymer chains. At the same time, TEOS may have formed dense silica nanoparticles by itself via hydrolysis, as in the Stöber process. Therefore, two distinct predominant particle sizes may have been observed as 222 nm and 40 nm. Other size distribution graphs along the sampling process can be found respectively below.

Table 7.2 Size distribution of nanoparticles via DLS

M_w	PolyH in EtOH (nm)	PdI	Pre-Reflux (nm)		PdI	Post Reflux (nm)		PdI	Post stock solution (nm)		PdI
Sol2 10k	91.32	0.198	31.38	236.3	0.531	260.2	34.74	0.503	222.9	40.22	0.499
Sol2 5k	36.88	0.162	70.97		0.106	70.80		0.129	83.62		0.084
Sol1 10k	507.1	0.586	121.6		0.238	183.4		0.215	183.9		0.152
Sol1 5k	423.0	0.542	239.6		0.088	163.8		0.130	180.5		0.124

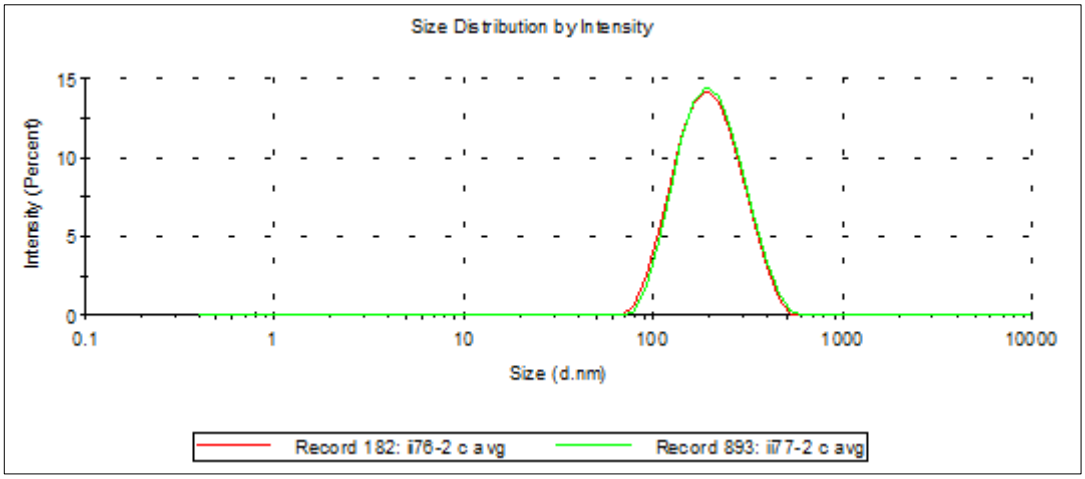

Figure 7.33 Sol1 5k (red), Sol1 10k (green) post stock solution particle size distribution graph

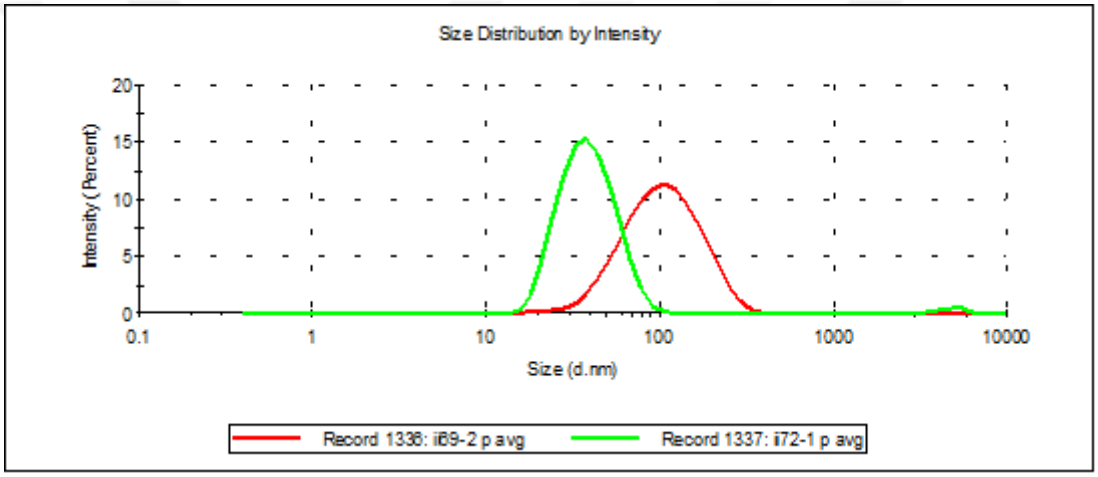

Figure 7.34 Sol2 5k (green), Sol2 10k (red) PolyH in EtOH particle size distribution graph

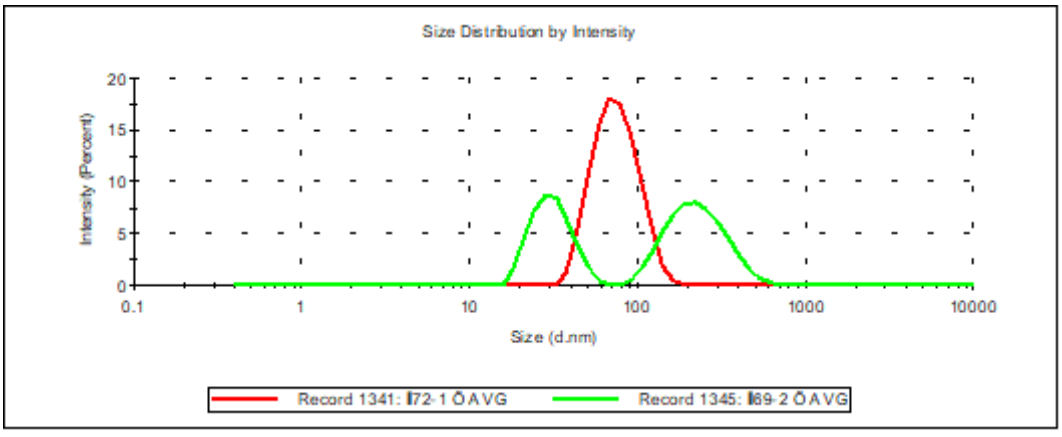

Figure 7.35 Sol2 5k (red), Sol2 10k (green) after TEOS addition particle size distribution graph

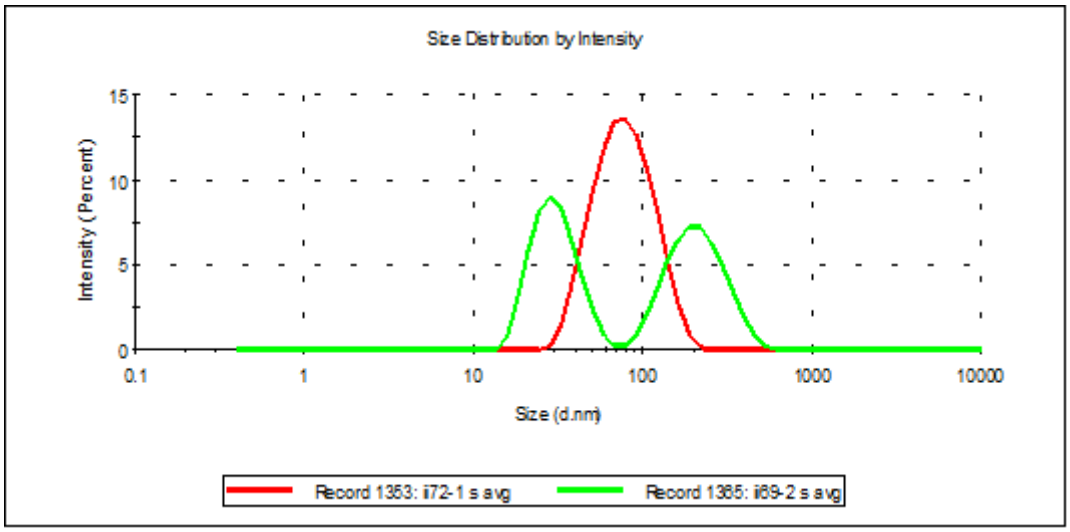

Figure 7.36 Sol2 5k (red), Sol2 10k (green) post reflux particle size distribution graph

According to the characterizations made from the prepared sol-gels, the coatings made from Sol1-5k and Sol2-5k were examined by SEM lateral section and UV spectrometer. DLS results of these sol-gels that make up these results are as in Figure 7.37 and Figure 7.38.

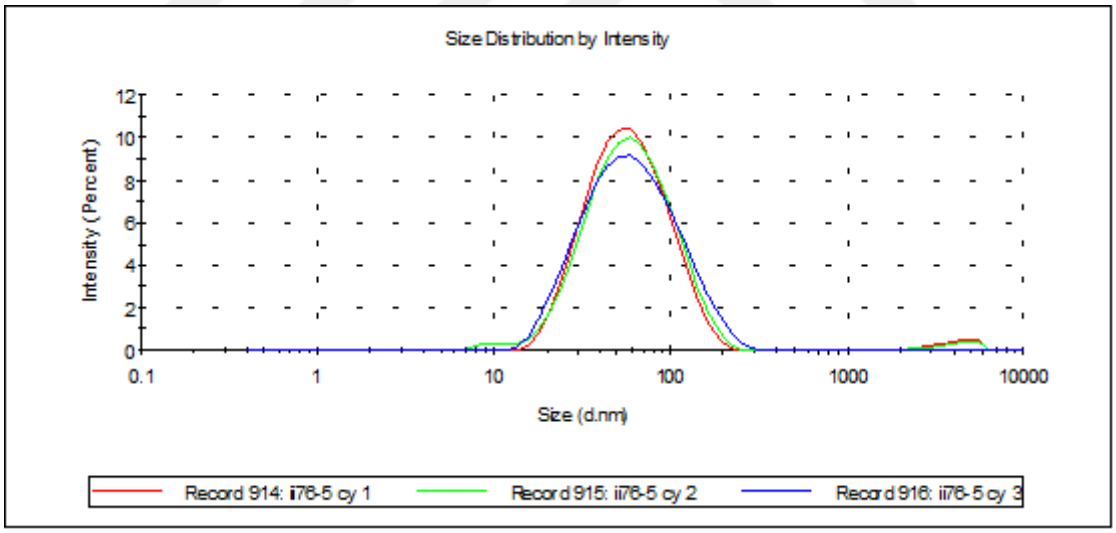

Figure 7.37 Sol1 5k post reflux particle size distribution graph

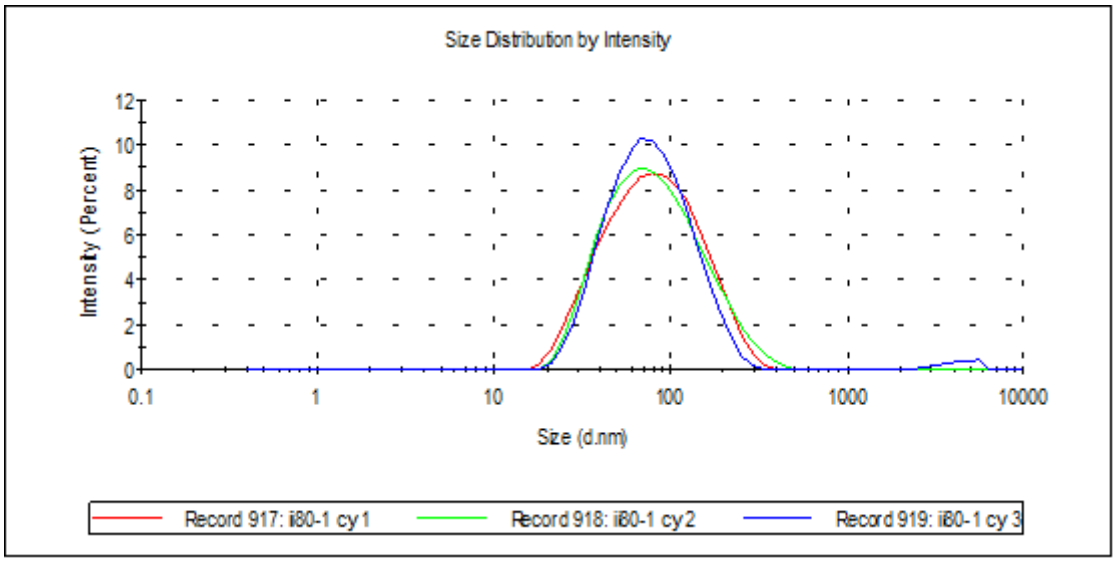

Figure 7.38 Sol2 5k post reflux particle size distribution graph

7.3.3 Nanoparticles Size Distribution via Transmission Electron Microscopy

In the literature there are some great examples of TEM imaging to core-shell templates. We took Wang's work as reference to make comparisons as it can be seen at Figure 1.4.

To prepare the samples for transmission electron microscopy (TEM) observations, sols were diluted in ethanol by sonication for 15 min, followed by adding onto carbon-coated copper grid and dried in air. Two samples were taken from each of the 4 different sol-gels prepared totalling 8 samples. One of these samples was taken when polymer dissolved in ammonia was added to ethanol medium. The other sample was taken after the stock solution was added to the medium. The aim of sampling of these two different steps is to see the polyelectrolyte template first and then see the SiO_2 shell around the polymer template. For both norbornene and oxanorbornene polymer templates the 5,000 g/mol molecular weighted ones (Figure 7.39 and Figure 7.41) have more uniform templates with nearly 30-40 nm diameter compared to 10,000 g/mol polymer used sol-gels (Figure 7.40 and Figure 7.42). There are some inconsistent results with DLS, Sol1 series has measured nearly 180 nm diameter while TEM images revealed actually, they have smaller nearly 50 nm diameter templates. As it can be seen in Figure 7.42 Sol2-

10k has probably aggregated before the imaging due to unstable structure of the sample clusters of the templates can be seen clearly.

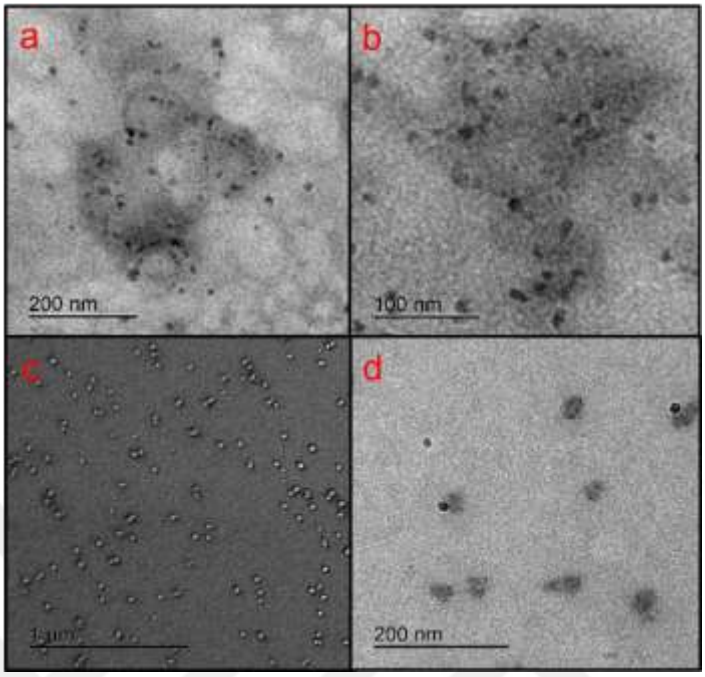

Figure 7.39 Sol1-5k TEM images a,b: PolyH in EtOH c,d: post stock solution

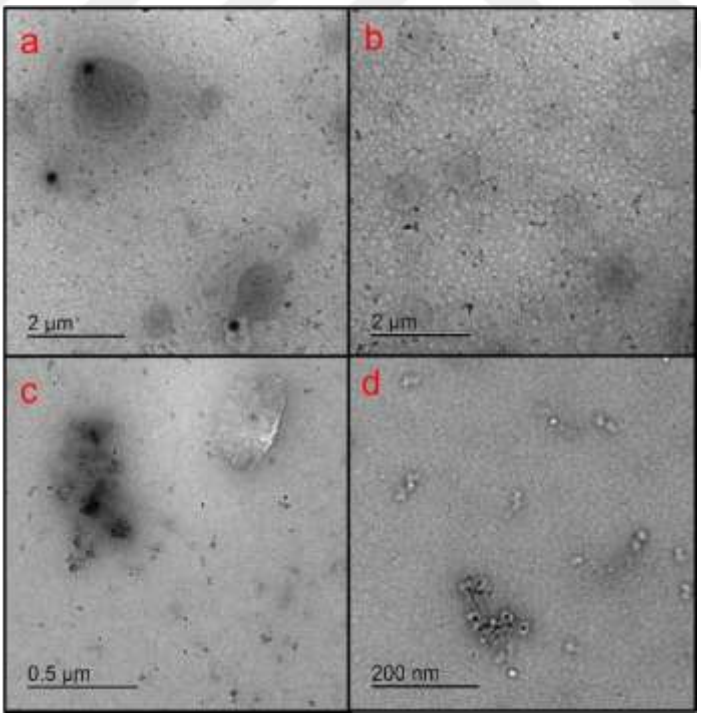

Figure 7.40 Sol1-10k TEM images a,b: PolyH in EtOH c,d: post stock solution

For Figure 7.41 the only the polymer structure is observed at a and b as expected. After TEOS was added to the medium, the SiO_2 shell structure formed successfully surrounded the polymer and enabled the core-shell structure to form. Particle size looks slightly smaller than measured in DLS which is 83 nm.

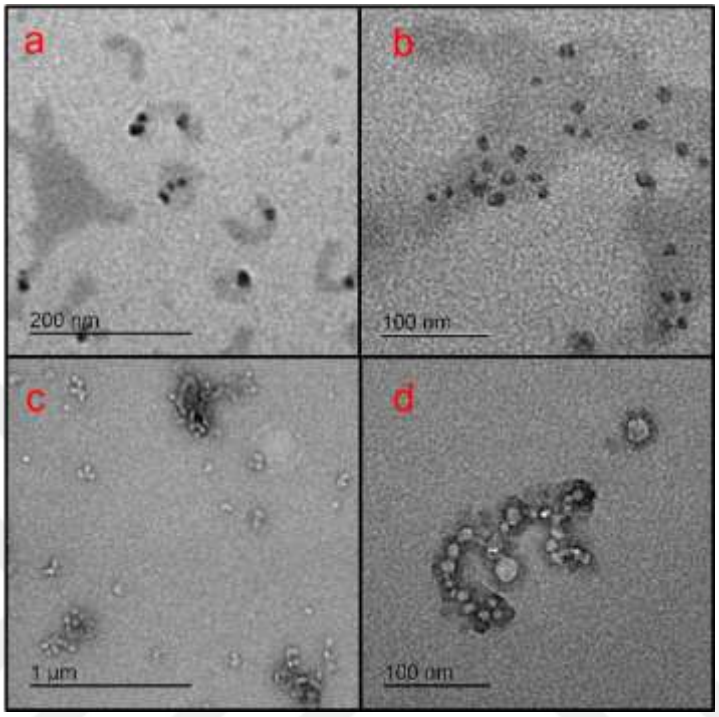

Figure 7.41 Sol2-5k TEM images a,b: PolyH in EtOH c,d: Post Stock solution

As it can be seen in Figure 7.42 Sol2-10k has probably aggregated before the imaging due to unstable structure of the sample in a and b. Clusters can be seen clearly in d. Core and shell template was not observed.

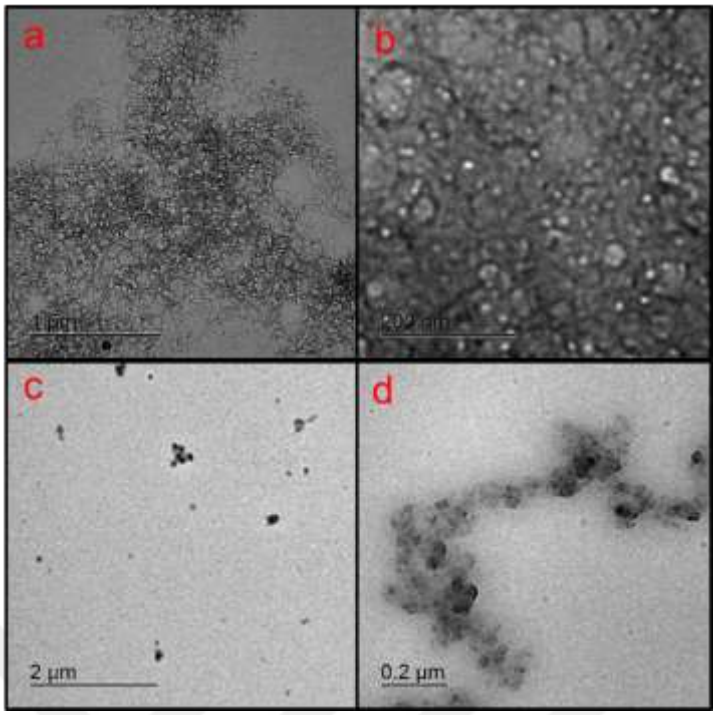

Figure 7.42 Sol2-10k TEM images a,b: PolyH in EtOH c,d: post stock solution

7.4 Coating with Produced Sol-Gels

7.4.1 Dip-coating Procedure with Produced Sol-Gels

With the prepared different sol-gels, using Dip Coater only one surface of the freshly cleaned glasses (4 x 10 cm^2) were coated. The glasses were immersed on the solution surface at an angle of 90° and constant velocity (Figure 7.43 left). The device is positioned in a closed cabin and the coating is done in ambient conditions. After the coating process of the glasses was completed, they were kept in the ambient conditions in the cabin for 10 minutes, then they were cured in an oven at 100 °C for 10 minutes and finally tempered in a high-temperature oven at 700 °C for 3 minutes.

Unfortunately, after tempering it is observed that coating was poorly held on to the glass surface. This may happen from two different reason, firstly the withdrawal rate is too slow, and coating became too thin to be observed. Second, sol-gel composition is not good enough to held on to the glass surface (Figure 7.43 right). The dip coating process was repeated several times to obtain a more uniform coating. For both polymer group, 5,000 g/mol molecular weighted sol-

gels held on to glass much more uniformly (Sol1-5k, Sol2-5k) compared to 10,000 g/mol polymer used sol-gels.

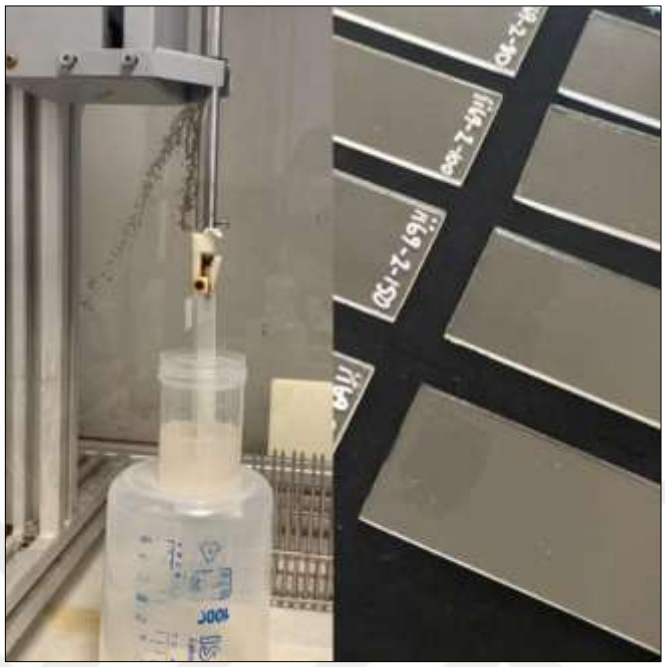

Figure 7.43 Dip-coater process (left) coated glasses (right)

7.4.2 Characterization of Coated Glasses

Using ASTM D1003 and ISO standards, the total transmission and haze measurements of all the coated glasses were made on the Haze meter. The results are given in Table 7.3 below only %1 increase in the transmission is obtained. The results showed that the increase in transmission was less than expected. The highest increase compared to the uncoated glass may be due to the fact that this coating does not adhere well to the glass, the adhered coating is thin, and therefore the nanoparticles cannot find enough space in the coating thickness.

Table 7.3 %Transmittance and %Haze measurements of coated glasses

Reaction Code	Withdrawing Rate (mm/min)	% Transmittance	% Haze
Sol1-5k	50	91.9	3.33
	80	92.0	3.72
	100	92.0	4.19
	150	90.9	6.57
	200	92.8	6.09

Table 7.4 %Transmittance and %Haze measurements of coated glasses (continued)

	50	**92.0**	**2.0**
	80	91.9	3.03
Sol1-10k	100	92.0	2.69
	150	91.8	4.88
	200	91.8	4.91
	50	91.8	3.38
	80	91.8	3.33
Sol2-5k	100	91.7	3.50
	150	92.6	2.63
	200	92.7	2.87
	50	91.7	6.16
	80	91.7	4.33
Sol2-10k	100	91.8	3.04
	150	92.3	5.38
	200	91.8	6.57
Bare Glass	**-**	**91.8**	**0.99**

Based on the coated glass % transmission results, the samples with the highest transmission were measured in the UV-spectrometer as seen in Figure 7.44. The graph shows there is only a slight difference in the transmission between these two different polymers cored coating solutions. Compared to uncoated bare glass transmission, %0.9 increasement observed in Sol1-5k-200 with the peak point at 545 nm wavelength. Also with a slight difference, Sol2-5k-200 %0.8 increasement in transmittance observed with the peak point at 545 nm wavelength.

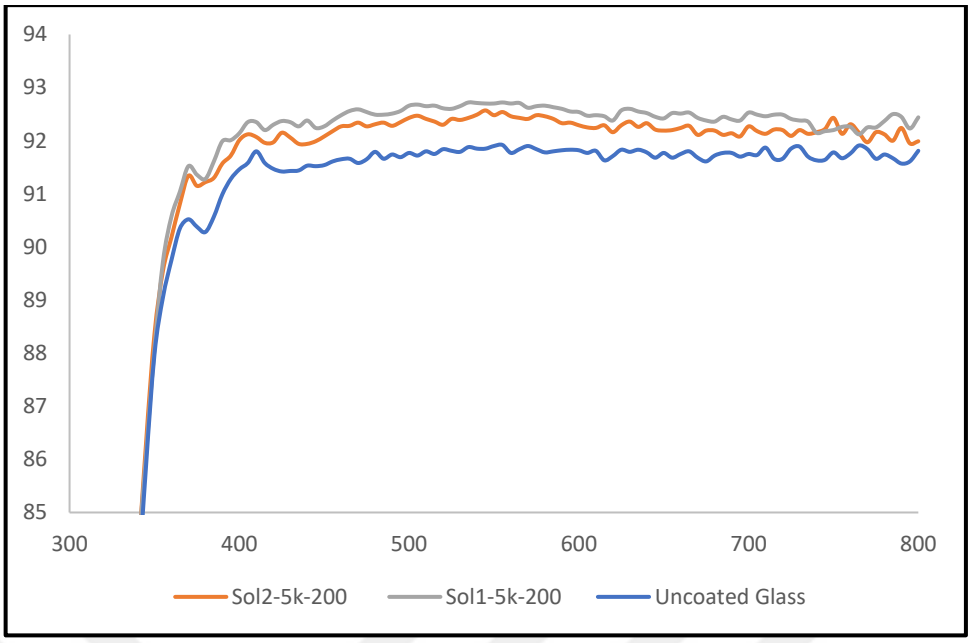

Figure 7.44 Coated glass transmission graph of Sol1-5k-200 and Sol2-5k-200

Sol1-5k-200 and Sol2-5k-200 glass samples are used for field emission scanning electron microscopy (FE-SEM)-cross section imaging. The cross-section samples were prepared by cutting the coated glass into $1cm^2$ from the coated part. The cutting process is done by diamond pencil and cut from the uncoated back side of the glass to avoid any damage to coating. After smoothing the side surfaces of it, coated with gold, and examined under vacuum condition. The images showed that the Sol1-5k have more uniform coating than Sol2-5k in Figure 7.45 and Figure 7.46. In Figure 7.45 the expected pores are observed in 70 nm coating thickness as with 15 to-30 nm core radius. But in Figure 7.46 there is no pore observation due to the nonuniform coating thickness.

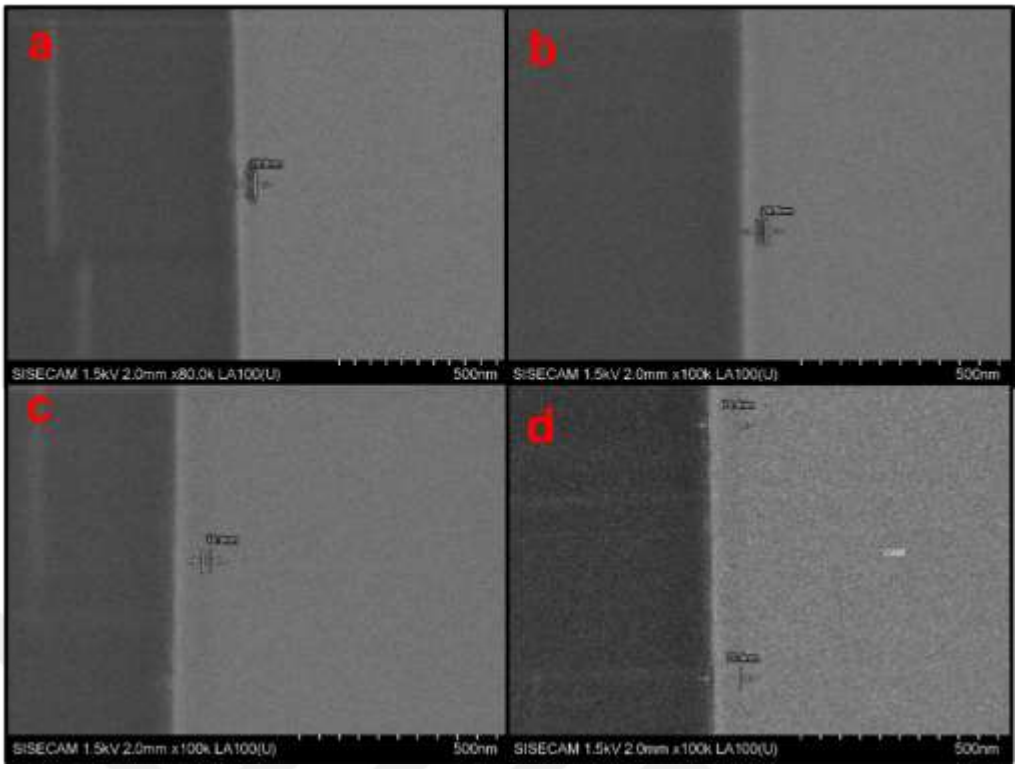

Figure 7.45 FE-SEM cross-section images of Sol1-5k-200

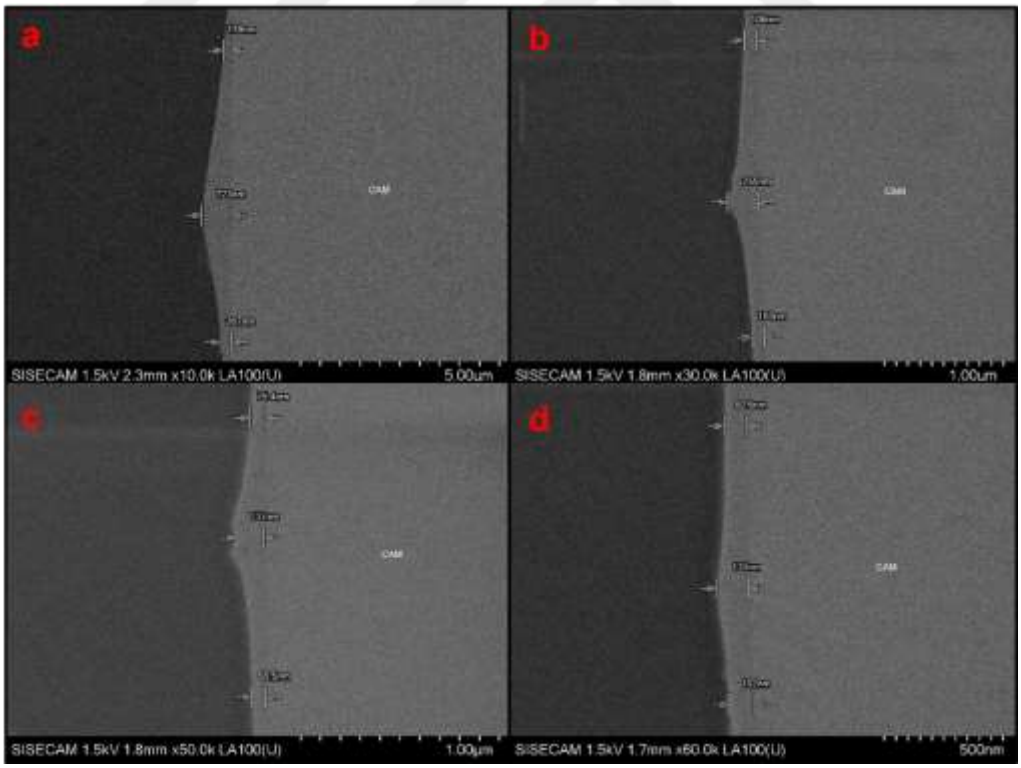

Figure 7.46 FE-SEM cross-section images of Sol2-5k-200

7.5 Conclusion

In this study, carboxylic acid functional ROMP homopolymers (norbornene and oxanorbornene series) with molecular weights of 5,000 g/mol and 10,000 g/mol were synthesized from 2 different monomers. Characterization of synthesized monomers and homopolymers was done by ^{1}H NMR, ^{13}C NMR, and FTIR. Although the anhydride rings of the synthesized polymers were tried to be opened with water first, successful results were not obtained, especially in oxanorbornene homopolymers. For this reason, in order to be the same in the whole study, the anhydride rings of all the synthesized polymers were opened using ammonia and turned into polyelectrolyte structures for use in sol-gels. These structures were characterized by ^{13}C NMR. By using these modified polymers to form core-shell structures, a total of 4 different sol-gels were prepared from each polymer and molecular weight group coded as Sol1-5k, Sol1-10k, Sol2-5k, Sol2-10k. These sol-gels were examined by DLS and TEM, as a result, it was seen that the core-shell templates prepared using 5,000 g/mol molecular weight norbornene and oxanorbornene based polymers formed more monodisperse, stable, spherical templates with 180 and 80 nm diameters respectively according to DLS results. Coating was done with the prepared sol-gels using the dip coating method on one surface and in a single layer. It was observed that the solutions used in the coatings did not adhere well to the glass. The coated glasses were characterized by UV-spectrometry and FE-SEM. In the FE-SEM cross-section examination, the targeted porous structure was successfully observed in the coating made with sol-gel prepared using *Exo*-Norbornene polymer with a molecular weight of 5,000 g/mol, although the porous structure was few in number. It has been observed that the transmittance of the glass can be increased by a maximum of 1% after polynorbornene based coatings . This increase was observed in the glass sample with porosity observed in FE-SEM. Although this increase is not sufficient for a coating that is expected to have anti-reflective properties, it is predicted that higher transmittance increases can be achieved in the sol-gel prepared in further studies, by strengthening the matrix with the addition of stock solution, by

developing further optimization studies on withdrawal speeds during dip-coating, and by making follow-up studies.

REFERENCES

[1] B. Parida, S. Iniyan, and R. Goic, "A review of solar photovoltaic technologies," *Renewable and Sustainable Energy Reviews*, vol. 15, no. 3, pp. 1625–1636, Apr. 2011, doi: 10.1016/J.RSER.2010.11.032.

[2] L. el Chaar, L. A. Lamont, and N. el Zein, "Review of photovoltaic technologies," *Renewable and Sustainable Energy Reviews*, vol. 15, no. 5, pp. 2165–2175, Jun. 2011, doi: 10.1016/J.RSER.2011.01.004.

[3] E. Lorenzo, "On the historical origins of bifacial PV modelling," *Solar Energy*, vol. 218, pp. 587–595, Apr. 2021, doi: 10.1016/J.SOLENER.2021.03.006.

[4] "Güneş Panelinin Tarihçesi - BFI Solar Enerji | Ordu." https://www.bfi.com.tr/gunes-panelinin-tarihcesi/ (accessed Jan. 23, 2023).

[5] "History and the Development of Photovoltaics - AE Solar." https://ae-solar.com/history-of-solar-module/ (accessed Jan. 23, 2023).

[6] P. T. Tanev, Y. Liang, and T. J. Pinnavaia, "Assembly of Mesoporous Lamellar Silicas with Hierarchical Particle Architectures," *J Am Chem Soc*, vol. 119, no. 37, pp. 8616–8624, Sep. 1997, doi: 10.1021/JA970228V.

[7] Y. Wan and S. H. Yu, "Polyelectrolyte controlled large-scale synthesis of hollow silica spheres with tunable sizes and wall thicknesses," *Journal of Physical Chemistry C*, vol. 112, no. 10, pp. 3641–3647, Mar. 2008, doi: 10.1021/jp710990b.

[8] Y. Nakashima, C. Takai, H. Razavi-Khosroshahi, and M. Fuji, "Influence of the PAA concentration on PAA/NH3 emulsion template method for synthesizing hollow silica nanoparticles," *Colloids Surf A Physicochem Eng Asp*, vol. 546, pp. 301–306, Jun. 2018, doi: 10.1016/J.COLSURFA.2018.03.033.

[9] Z. Q. Guo, Y. Liu, M. Y. Tang, J. H. Wang, and X. P. Su, “Super-durable closed-surface antireflection thin film by silica nanocomposites,” *Solar Energy Materials and Solar Cells*, vol. 170, pp. 143–148, Oct. 2017, doi: 10.1016/j.solmat.2017.05.043.

[10] X. Zhang *et al.*, “Multifunctional antireflection coatings based on novel hollow silica-silica nanocomposites,” *ACS Appl Mater Interfaces*, vol. 6, no. 3, pp. 1415–1423, Feb. 2014, doi: 10.1021/AM405258D/SUPPL_FILE/AM405258D_SI_002.AVI.

[11] P. Buskens, M. Burghoorn, M. C. D. Mourad, and Z. Vroon, “Antireflective Coatings for Glass and Transparent Polymers,” *Langmuir*, vol. 32, no. 27, f10.1021/ACS.LANGMUIR.6B00428/ASSET/IMAGES/MEDIUM/LA-2016-00428C_0017.GIF.

[12] Z. W. Han *et al.*, “Antireflective surface inspired from biology: A review,” *Biosurf Biotribol*, vol. 2, no. 4, pp. 137–150, Dec. 2016, doi: 10.1016/J.BSBT.2016.11.002.

[13] L. Klein, M. Aparicio, and A. Jitianu, “Handbook of Sol-Gel Science and Technology.”

[14] H. K. Raut, V. A. Ganesh, A. S. Nair, and S. Ramakrishna, “Anti-reflective coatings: A critical, in-depth review,” *Energy Environ. Sci.*, vol. 4, no. 10, pp. 3779–3804, 2011, doi: 10.1039/C1EE01297E.

[15] L. Yao and J. He, “Recent progress in antireflection and self-cleaning technology – From surface engineering to functional surfaces,” *Prog Mater Sci*, vol. 61, pp. 94–143, 2014, doi: https://doi.org/10.1016/j.pmatsci.2013.12.003.

[16] B. E. Yoldas, “Investigations of porous oxides as an antireflective coating for glass surfaces,” *Applied Optics, Vol. 19, Issue 9, pp. 1425-1429*, vol. 19, no. 9, pp. 1425–1429, May 1980, doi: 10.1364/AO.19.001425.

[17] *Sol-Gel Technologies for Glass Producers and Users*. Springer US, 2004. doi: 10.1007/978-0-387-88953-5.

[18] J. D. Wright and N. A. J. M. Sommerdijk, “Sol-Gel Materials : Chemistry and Applications,” *Sol-Gel Materials*, Oct. 2018, doi: 10.1201/9781315273808.

[19] S. S. Kistler, “Coherent Expanded Aerogels and Jellies,” *Nature 1931 127:3211*, vol. 127, no. 3211, pp. 741–741, 1931, doi: 10.1038/127741a0.

[20] S. S. Kistler, “Coherent expanded aerogels,” *Journal of Physical Chemistry*, vol. 36, no. 1, pp. 52–64, 1932, doi: 10.1021/J150331A003/ASSET/J150331A003.FP.PNG_V03.

[21] R. ROY, “Aids in Hydrothermal Experimentation: II, Methods of Making Mixtures for Both ‘Dry’ and ‘Wet’ Phase Equilibrium Studies,” *Journal of the American Ceramic Society*, vol. 39, no. 4, pp. 145–146, Apr. 1956, doi: 10.1111/J.1151-2916.1956.TB14180.X.

[22] R. ROY, “Gel Route to Homogeneous Glass Preparation,” *Journal of the American Ceramic Society*, vol. 52, no. 6, pp. 344–344, Jun. 1969, doi: 10.1111/J.1151-2916.1969.TB11945.X.

[23] S. H, “Oxide layers deposited from organic solutions.,” *Phys Thin Films*, vol. 5, pp. 87–141, 1969, Accessed: Oct. 25, 2022. [Online]. Available: https://jglobal.jst.go.jp/en/detail?JGLOBAL_ID=201602009922044869

[24] H. Dislich, “New Routes to Multicomponent Oxide Glasses,” *Angewandte Chemie International Edition in English*, vol. 10, no. 6, pp. 363–370, Jun. 1971, doi: 10.1002/ANIE.197103631.

[25] W. Stöber, A. Fink, and E. Bohn, “Controlled growth of monodisperse silica spheres in the micron size range,” *J Colloid Interface Sci*, vol. 26, no. 1, pp. 62–69, Jan. 1968, doi: 10.1016/0021-9797(68)90272-5.

[26] M. Nabavi, S. Doeuff, C. Sanchez, and J. Livage, “31 North-Holland Chemical Modification Of Metal Alkoxides By Solvents: A Way To Control Sol-Gel Chemistry,” 1990.

[27] C. W. Turner, “Sol-gel process-principles and applications,” *undefined*, 1991.

[28] L. P. Singh *et al.*, “Sol-Gel processing of silica nanoparticles and their applications,” *Adv Colloid Interface Sci*, vol. 214, pp. 17–37, Dec. 2014, doi: 10.1016/J.CIS.2014.10.007.

[29] C. Milea, C. Bogatu, and A. Duta, “The influence of parameters in silica sol-gel process,” *Bull Trans Univer Braşov ser i Eng Sci*, vol. 4, Oct. 2011.

[30] M. v. Landau, “Sol-Gel Process,” *Handbook of Heterogeneous Catalysis*, Jan. 2008, doi: 10.1002/9783527610044.HETCAT0009.

[31] C. McDonagh, F. Sheridan, T. Butler, and B. D. MacCraith, “Characterisation of sol-gel-derived silica films,” *J Non Cryst Solids*, vol. 194, no. 1–2, pp. 72–77, Jan. 1996, doi: 10.1016/0022-3093(95)00488-2.

[32] T. M. Butler, B. D. MacCraith, and C. McDonagh, “Leaching in sol–gel-derived silica films for optical pH sensing,” *J Non Cryst Solids*, vol. 224, no. 3, pp. 249–258, 1998, Accessed: Oct. 29, 2022. [Online]. Available: https://www.academia.edu/38105961/Leaching_in_sol_gel_derived_silica_films_for_optical_pH_sensing

[33] Ş. Toygun, G. Köneçoğlu, and Y. Kalpaklı, “General principles of sol-gel,” *Sigma*, vol. 31, pp. 456–476, Oct. 2013.

[34] G. Aydin, M. Bilimi, M. Anabilim, D. Malzeme, B. ve, and M. Programı, “İstanbul Teknik Üniversitesi ↔ Fen Bilimleri Enstitüsü Yüksek Lisans Tezi Tek Katmanli Yansima Önleyici İnce Film Kaplamalarin Üretimi ve Optik/Mekanik Özelliklerinin İncelenmesi.”

[35] W. Stöber, A. Fink, and E. Bohn, “Controlled growth of monodisperse silica spheres in the micron size range,” *J Colloid Interface Sci*, vol. 26, no. 1, pp. 62–69, Jan. 1968, doi: 10.1016/0021-9797(68)90272-5.

[36] “Stöber process - Wikipedia.” https://en.wikipedia.org/wiki/St%C3%B6ber_process (accessed Jan. 23, 2023).

[37] G. H. Bogush, M. A. Tracy, and C. F. Zukoski IV, “Preparation of monodisperse silica particles: Control of size and mass fraction,” *J Non Cryst*

Solids, vol. 104, no. 1, pp. 95–106, Aug. 1988, doi: 10.1016/0022-3093(88)90187-1.

[38] T. Gholami, M. Salavati-Niasari, M. Bazarganipour, and E. Noori, "Synthesis and characterization of spherical silica nanoparticles by modified Stöber process assisted by organic ligand," *Superlattices Microstruct*, vol. 61, pp. 33–41, Sep. 2013, doi: 10.1016/J.SPMI.2013.06.004.

[39] M. Saçak, *Polimer kimyası*. Gazi kitapevi, 2008.

[40] J. R. Fried, *Polymer Science and Technology*, Third Edition. 2014.

[41] LG. Wade, *Organic chemistry*, 8th ed. New York: Pearson Education, 2012.

[42] M. Szwarc, "Living polymers. Their discovery, characterization, and properties," *Journal of Polymer Science Part A*, 1998, doi: 10.1002/(SICI)1099-0518(19980115)36:1.

[43] M. Stevens, *Polymer chemistry*. New York: Oxford University Press, 1990.

[44] K. Matyjaszewski, "Controlled Radical Polymerization: State of the Art in 2008," 2009, Accessed: Jan. 09, 2023. [Online]. Available: https://pubs.acs.org/sharingguidelines

[45] P. Dubois, Olivier. Coulembier, and J.-Marie. Raquez, *Handbook of ring-opening polymerization*. Wiley-VCH, 2009.

[46] S. Hilf and A. F. M. Kilbinger, "Functional end groups for polymers prepared using ring-opening metathesis polymerization," *Nat Chem*, vol. 1, no. 7, pp. 537–546, Oct. 2009, doi: 10.1038/nchem.347.

[47] R. H. Grubbs and E. Khosravi, "Edited by Handbook of Metathesis Volume 3: Polymer Synthesis."

[48] C. W. Bielawski and R. H. Grubbs, "Living ring-opening metathesis polymerization," *Prog Polym Sci*, vol. 32, no. 1, pp. 1–29, Jan. 2007, doi: 10.1016/J.PROGPOLYMSCI.2006.08.006.

[49] C. W. Bielawski and R. H. Grubbs, “Living ring-opening metathesis polymerization,” *Prog Polym Sci*, vol. 32, no. 1, pp. 1–29, Jan. 2007, doi: 10.1016/J.PROGPOLYMSCI.2006.08.006.

[50] “Yildiz Teknik Üniversitesi Fen Bilimleri Enstitüsü Fosfonyum Gruplari Içeren Romp Polimerlerinin Sentezi, Karakterizasyonu Ve Antibakteriyel Etkinliklerinin Incelenmesi.”

[51] C. A. Citron, S. M. Wickel, B. Schulz, S. Draeger, and J. S. Dickschat, “A Diels–Alder/Retro-Diels–Alder Approach for the Enantioselective Synthesis of Microbial Butenolides,” *European J Org Chem*, vol. 2012, no. 33, pp. 6636–6646, Nov. 2012, doi: 10.1002/EJOC.201200991.

[52] “The C=O Bond, Part IV: Acid Anhydrides.” https://www.spectroscopyonline.com/view/co-bond-part-iv-acid-anhydrides (accessed Jan. 23, 2023).

[53] M. W. Lee and W. C. Herndon, “Stereochemistry of the Furan-Maleic Anhydride Cycloaddition,” *Journal of Organic Chemistry*, vol. 43, no. 3, p. 518, 1978, doi: 10.1021/JO00397A031/ASSET/JO00397A031.FP.PNG_V03.

[54] J. xing Yang, L. xia Ren, and Y. sheng Li, “Ring-opening metathesis polymerization of cis-5-norbornene-endo-2,3-dicarboxylic anhydride derivatives using the grubbs third generation catalyst,” *Chinese Journal of Polymer Science (English Edition)*, vol. 35, no. 1, pp. 36–45, Jan. 2017, doi: 10.1007/S10118-017-1873-1/METRICS.

[55] C. W. Bielawski, D. Benitez, T. Morita, and R. H. Grubbs, “Synthesis of end-functionalized poly(norbornene)s via ring-opening methathesis polymerization,” *Macromolecules*, vol. 34, no. 25, pp. 8610–8618, Dec. 2001, doi: 10.1021/MA010878Q/SUPPL_FILE/MA010878Q_S.PDF.

[56] B. Yang, B. A. Abel, C. L. McCormick, and R. F. Storey, “Synthesis of Polyisobutylene Bottlebrush Polymers via Ring-Opening Metathesis Polymerization,” *Macromolecules*, vol. 50, no. 19, pp. 7458–7467, Oct.

2017, doi: 10.1021/ACS.MACROMOL.7B01655/SUPPL_FILE/MA7B01655_SI_001.PDF.

[57] O. L. Torres-Rocha, X. Wu, C. Zhu, C. M. Crudden, and M. F. Cunningham, “Synthesis of Diblock and Triblock Polymers from Cyclooctadiene and Norbornene Via ROMP in Miniemulsion,” *Macromol Rapid Commun*, vol. 40, no. 13, Jul. 2019, doi: 10.1002/MARC.201900087.

[58] J. D. Rule and J. S. Moore, “ROMP reactivity of endo- and exo-dicyclopentadiene,” *Macromolecules*, vol. 35, no. 21, pp. 7878–7882, Oct. 2002, doi: 10.1021/MA0209489.

[59] “Zetasizer Nano User Manual MAN0485,” no. Issue 1.1. Malvern Instruments Ltd., Worcestershire, United Kingdom, pp. 215–223, Apr. 2013.

[60] R. H. Ebini and C. M. Sorensen, “Light scattering studies of the sol-to-gel transition in particulate systems,” *J Colloid Interface Sci*, vol. 556, pp. 577–583, Nov. 2019, doi: 10.1016/J.JCIS.2019.08.075.

[61] L. Chen, Z. Li, P. Zhang, P. Tian, J. Yuan, and W. Zheng, “Effect of PAA on the structure and transmittance of hollow spherical SiO2 film prepared by sol-gel method,” *Ceram Int*, Nov. 2022, doi: 10.1016/j.ceramint.2022.11.089.

PUBLICATIONS FROM THE THESIS

O.I. Irey, M. Gallei, R. Budakoğlu, T. Eren “Anti-reflektif Kaplamalara Yönelik Silika Polinorbornen Nanokompozitlerin Sentezi”, presented at the 34th Ulusal Kimya Kongresi, Yalova, Turkey, Sep. 1-6, 2022, PS-170